Bioactive Materials 43 (2025) 67–81

Contents lists available at ScienceDirect

Bioactive Materials

journal homepage: www.keaipublishing.com/en/journals/bioactive-materials

Immune-modulative nano-gel-nano system for patient-favorable cancer therapy

Sung Hoon Kim [a], Rafael T. Han [b,c,d], Hyung-Seop Han [a], Young-Min Kim [a,d,*]

[a] Biomaterials Research Center, Korea Institute of Science and Technology (KIST), Seoul, 02792, Republic of Korea
[b] Chemical and Biomedical Integrative Research Center, Korea Institute of Science and Technology (KIST), Seoul, 02792, Republic of Korea
[c] KHU-KIST Department of Converging Science and Technology, Kyung Hee University, Seoul 02447, Republic of Korea
[d] Division of Biomedical Science and Technology, KIST School, Korea University of Science and Technology, Seoul, 02792, Republic of Korea

ARTICLE INFO

Keywords:
Injectable hydrogel
Multi-targetable
Nanocomplexes
Patient-favorable
In situ cancer vaccine

ABSTRACT

Current cancer immunotherapies exhibit low response rates attributed to suppressive tumor immune microenvironments (TIMEs). To address these unfavorable TIMEs, supplementation with tumor-associated antigens and stimulation of immune cells at target sites are indispensable for eliciting anti-tumoral immune responses. Previous research has explored the induction of immunotherapy through multiple injections and implants; however, these approaches lack consideration for patient convenience and the implementation of finely tunable immune response control systems to mitigate the side effects of over-inflammatory responses, such as cytokine storms. In this context, we describe a patient-centric nano-gel-nano system capable of sustained generation of tumor-associated antigens and release of adjuvants. This is achieved through the specific delivery of drugs to cancer cells and antigens/adjuvants to immune cells over the long term, maintaining proper concentrations within the tumor site with a single injection. This system demonstrates local immunity against tumors with a single injection, enhances the therapeutic efficacy of immune checkpoint blockades, and induces systemic and memory T cell responses, thus minimizing systemic side effects.

1. Introduction

Cancer immunotherapy activates and trains the immune systems of patients to attack cancer cells and has, therefore, garnered much attention in oncology over the last decade [1,2]. However, only a small subset of patients with malignant tumors (5–30 %) respond to a representative drug, immune checkpoint blockade (ICB) treatment in clinical trials [3–6]. This is because of the suppressive tumor immune microenvironment (TIME) with low levels of cytotoxic T cells against the tumor and the high expression of immunosuppressive factors [7–9]. To transform the suppressed TIMEs, antigens, and adjuvants should be delivered to the antigen-presenting cells (APCs) which subsequently induce antigen-specific T cell responses [10,11].

Therapeutic cancer vaccination is an anticancer immunotherapeutic strategy that generates tumor-specific immune responses to recapture the control of tumor growth and eradicate residual cancer [12]. The basic concept required for a successful therapeutic cancer vaccine is to deliver both antigens and adjuvants to antigen-presenting cells (APCs) such as macrophages and dendritic cells (DCs), which subsequently induce antigen-specific T cell responses [13,14]. Among these antigens, *in situ* tumor-associated antigens (TAAs), generated directly from a patient's tumor using conventional chemotherapy, are in the spotlight because they instantaneously generate patient-specific immune responses to handle immunogenic mutations for personalized therapy with low side effects [15–17]. Adjuvants, small molecules that mimic pathogen invasion or cell damage, such as Toll-like receptor (TLR) agonists, are also delivered to APCs to enhance immune responses and induce cytotoxic T cells against tumors [18]. Most researchers have shown regressed tumor growth using a combination of antigens and adjuvants via surgical implants and intravenous administration with high doses, however it could negatively affect the patient's condition, resulting in immune environment changes with low therapeutic efficiency [19–21]. Moreover, multiple and invasive manners of administration might result in a low patient quality of life and induction of immune-suppressive responses [22]. Thus, intratumorally injected biomaterials as a drug delivery system have received substantial attention

Peer review under responsibility of KeAi Communications Co., Ltd.
* Corresponding author. Center of biomaterials, Korea Institute of Science and Technology (KIST), Seoul, 02792, Republic of Korea.
E-mail address: davidkim@kist.re.kr (Y.-M. Kim).

https://doi.org/10.1016/j.bioactmat.2024.08.047
Received 2 January 2024; Received in revised form 29 July 2024; Accepted 31 August 2024

in recent years because of the delivery of various vaccine drugs with proper concentrations in the local tumor site to increase therapeutic efficiency [23,24]. However, because naked drugs released from materials can be diffused and delivered into cells in TIMEs randomly, off-targeted delivery-mediated low therapeutic effects and side effects could be observed [16,25]. Therefore, strategies to sequentially target specific cells and cellular uptake mechanisms of the released drugs, reduce side effects due to over-immune responses, enhance therapeutic efficacy at local tumor sites consisting of various types of cells, and control patient-specific doses are desirable.

Herein, we propose an Arg-Gly-Asp (RGD)-Cationic (RC) peptide-conjugated poly (organophosphazene) (RCP) as a polymeric nanocomplex system capable of delivering multiple drugs into a local solid tumor for an extended period with an intratumoral injection. At low temperatures, the polymeric solution induces the formation of nano-sized complexes with poorly soluble paclitaxel (PTX) and anionic cytosine–phosphate–guanine motifs (CpG) through hydrophobic and ionic interactions, allowing for easy control of drug concentrations for patient-tailored therapy. It exhibits temperature-dependent sol-gel transitions at the target site following intratumoral injection. Subsequently, the drug-incorporated nanocomplexes were slowly released from a solidified gel at the center of the tumor site through dissolution and degradation over an extended period. Accordingly, we suggest "nanocomplex-hydrogel-nanocomplex (nano-gel-nano, NGN)" to explain the three steps of the RCP phase transition in this study, as illustrated in Fig. 1. Furthermore, the NGN system offers the benefit of preferentially delivering the released nanocomplexes into cancer cells through receptor-mediated endocytosis as well as passive delivery to antigen-presenting cells (APCs) without overdose-mediated adverse effects. The hydrogel system could consequently induce local innate-adaptive immune responses and modulate suppressed TIMEs by priming tumor-specific T cells, resulting in synergistic therapeutic efficacy with ICB, as well as preventing tumor recurrence and metastasis for an extended period with only a single administration. Therefore, NGN provides an effective cancer vaccine as local immune modulation, shows synergistic therapeutic efficacy with ICB, and prevents tumor recurrence and metastasis by systemically priming tumor-specific T cells, which could be useful in a patient-friendly approach with minimal invasiveness and frequency of administration (Fig. 1).

2. Material and methods

2.1. Materials

Hexachlorocyclotriphosphazene (Sigma Aldrich, Saint Louis, MO, USA) was purified by sublimation at 55 °C under vacuum (about 0.1 mmHg). Poly (dichlorophosphazene) was prepared as described previously [26]. It was prepared from hexachlorocyclotriphosphazene using aluminum chloride ($AlCl_3$) as a catalyst at 250 °C for 5 h. α-Amino--ω-methoxy-poly (ethylene glycol)s with molecular weights of 750 Da were prepared according to the literature [27]. L-Isoleucine ethyl ester hydrochloride (IleOEt·HCl) was purchased from A&Z Food Additives (HangZhou, China). 2-aminoethyl methacrylate was purchased from Polysciences. RC peptide (sequence: SDGRGGGGHHHHHHRRRRC) was purchased from GL Biochem (Shanghai, China). Tetrahydrofuran (THF) and triethylamine (TEA) (Junsei Chemical Co., Ltd., Japan) were purified under dry nitrogen atmosphere by refluxing at the boiling point over sodium metal-benzophenone and barium oxide. Paclitaxel (PTX) was

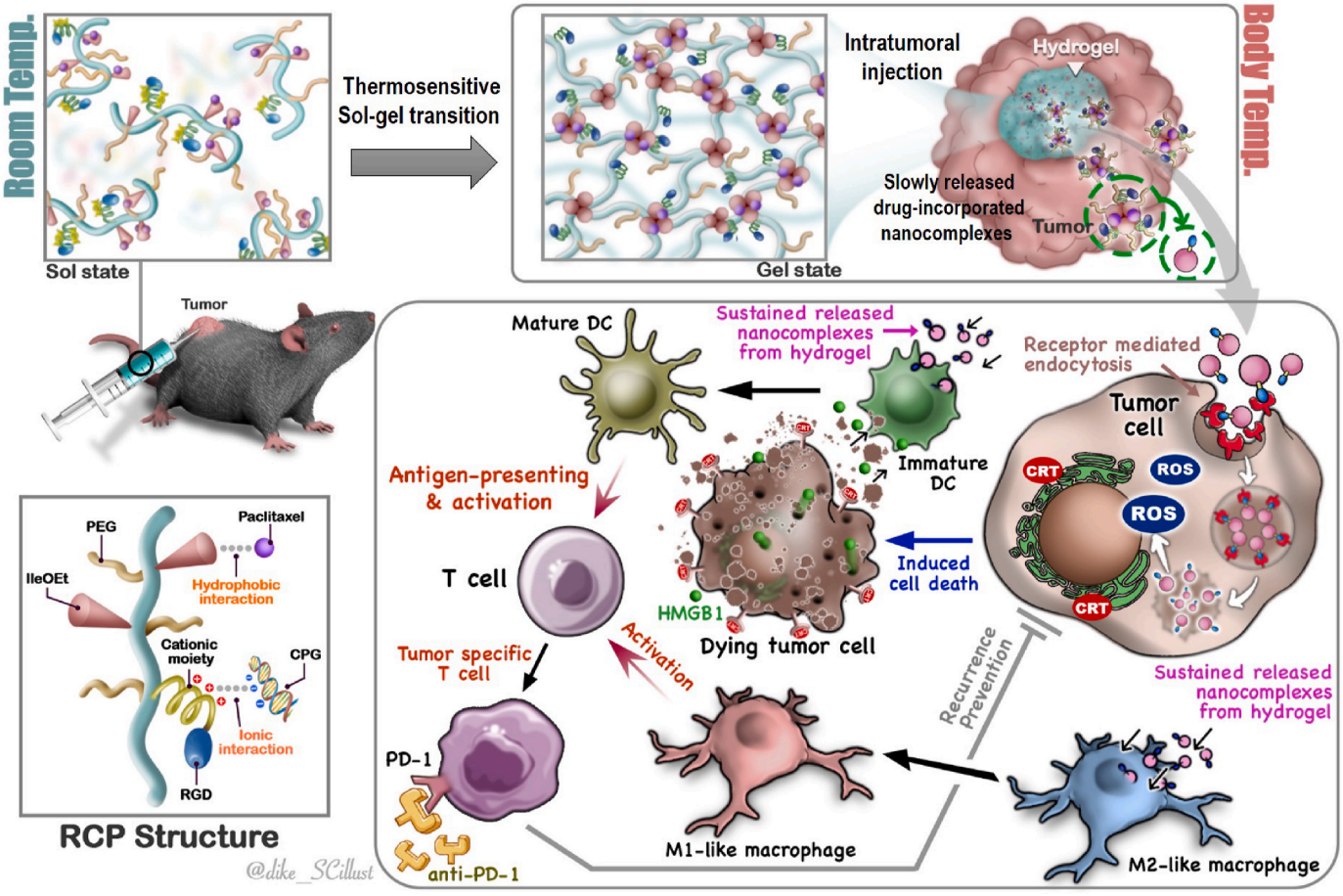

Fig. 1. Schematic illustration of a nano-gel-nano (NGN) system for local and long-term modulation of a suppressive TIME and enhancement of ICB therapeutic efficacy with a single injection for patient-favorable immunotherapy, including the mechanism underlying its action.

purchased from Selleck Chemicals. CpG-ODN 2395 (CpG) was purchased from Invivogen. αPD-1 (RMP1-14, InVivoMab anti-mouse PD-1) was purchased from BioXCell (West Lebanon, NH, USA).

2.2. Synthesis of methacrylated poly (organophosphazenes) [NP ($(IleOEt)_{1.22}$ $(MeAc)_{0.2}$ $(AMPEG750)_{0.58}$]

All reactions were carried out under an atmosphere of dry nitrogen using the standard Schlenk-line techniques. Polyphosphazenes with methacrylate moiety (Polymer 1 in Fig. S1) were synthesized as indicated below. IleOEt·HCl (23.3 g, 119.07 mmol) in dry tetrahydrofuran (THF) containing trimethylamine (TEA) was added slowly to poly (dichlorophosphazene) (10.00 g, 86.29 mmol) dissolved in dry THF. The reaction mixture was stirred in dry ice/acetone bath for 12 h and then at room temperature for 36 h. 2-amino ethyl methacrylate (4.29 g, 25.89 mmol) and AMPEG750 (41.42 g, 55.22 mmol) were dissolved in dry THF including TEA and added to the mixture. The reaction mixture was stirred at room temperature for 24 h and then at 40–50 °C for 24 h. AMPEG750 (18.76 g, 25.02 mmol) in dried THF was added to the reaction mixture and stirred at room temperature for 24 h and then at 40–50 °C for 24 h [28,29]. The polymer reaction mixture was purified as per our previous reports [30,31]. The reaction mixture was filtered, and the solvents were removed. Then, concentrated reaction mixture was poured into n-hexane to obtain a precipitate, which was re-precipitated twice in the same solvent system. The polymer product was further purified by dialysis with a dialysis membrane (Spectra/Por, MWCO: 10–12 kDa) against methanol for 4 days at room temperature and against distilled water for 4 days at 4 °C. The dialyzed solution was freeze-dried to obtain polymer (MePPZ). ^{1}H NMR (CDCl3, δ, ppm): 0.91–1.05 (s, 6H, -CH_3 and CH_2CH_3 of IleOEt), 1.05–1.40 (b, 3H, -OCH_2CH_3 of IleOEt), 1.40–1.62 (b, 2H, -CH_2CH_3 of IleOEt), 1.62–1.85 (b, 1H, -$CH(CH_3)CH_2CH_3$ of IleOEt), 1.8–2.05 (s, 3H, CH_2=$C(CH_3)$- of AEMA), 2.80–3.18 (b, 4H -$NHCH_2CH_2O$- of AMPEG and -NH-CH_2-CH_2- of AEMA), 3.38 (s, 3H, -CH_3 of AMPEG), 3.50–3.91 (b, 62H, -$(CH_2CH_2O)_{11}$- of AMPEG), 3.91–4.00 (b, 1H, -NHCH- of IleOEt), 4.11–4.40 (b, 4H, -OCH_2CH_3 of IleOEt and -NH-CH_2-CH_2- of AEMA), 5.54 (s, 1H CH_2)$C(CH_2)$- of AEMA), and 6.11 (s, 1H CH_2)$C(CH_3)$- of AEMA).

2.3. Conjugation of the RC peptide with the methacrylated polymer [NP ($(IleOEt)_{1.22}$ $(MeAc)_{0.14}$ $(AMPEG750)_{0.58}$ $(RC)_{0.06}$], RCP

The methacrylated polymer (5 g, 0.57 mmol) was dissolved in dried DMF. When completely dissolved in solvent, hexylamine (0.75 g, 7.43 mmol) and RC peptide (3.37 mg, 1.49 mmol) were added and stirred at room temperature for 24 h. Afterward, the solvent in the reacted solution was removed and purified by dialysis (Spectra/Por, MWCO: 10–12 kDa) with methanol and distilled water for 3 days. The dialyzed solution was freeze-dried to obtain polymer as the final product.

2.4. Preparation of the RCP hydrogel solution

The RCP polymer solution (10 wt%) dissolved in distilled water was used for experiments after filtration using 0.2 μm cellulose acetate syringe filter. In the experiments where RCP polymer solution had to be mixed with PTX or CpG, we prepared high concentrations of PTX (× 10) and CpG (× 5) dissolved in 10 % RCP solution and then diluted each solution as indicated.

2.5. Characterizations of structures and physical properties of the polymers

The structure of prepared polymers was defined by a ^{1}H NMR spectrometer (Varian Gemini-3000, Agilent Technologies) operating at 400 MHz in the Fourier transform mode with $CDCl_3$ and DMSO used as the solvent. The viscosity of the aqueous polymer solutions was measured by a Brookfield RVDV-III + viscometer between 5 and 50 °C under a fixed shear rate of 0.1. The measurements were carried out with a set spindle speed of 0.2 rpm and with a heating rate of 1 °C/min. The measurement of rheology was performed with a 10 % RCP solution using the rheometer (MSC 102, Anton Paar, DE). The procedure involved a politer temperature-controlled bottom plate and a 25.0 mm parallel plate measuring system with a gap length of 0.3 mm. The measurements were conducted at an oscillating frequency of 1 Hz and an oscillating strain of 0.1 %, at temperatures of 4 and 37 °C. The storage modulus (G′) and loss modulus (G″) were obtained using the instrument's software. The sizes and ζ-potentials of RCP, RCP-P, RCP-C and RCP-PC (RCP with PTX, CpG and PTX/CpG denoted as RCP-P, RCP-C, and RCP-PC, respectively) were measured by a Zetasizer Nano ZS (Malvern Instruments Ltd., Malvern, UK) at room temperature. The final concentration of samples was 10 μg/mL, and the samples were measured in triplicate.

2.6. Gel retardation test

A 1 μg of CpG was used for complexation at predetermined weight/weight (RCP/CpG) ratios. The induced nanocomplexes were loaded on 10 % polyacrylamide gels and electrophoresis was carried out at 100 mV. After 1 h, the gels were stained and visualized with the Safe shine blue (Biosesang) and observed by iBrightImagers (CL1500, Invitrogen, USA).

2.7. In vitro PTX and CpG release from RCP hydrogel

Both RCP-P and RCP-C hydrogel solutions were prepared with PBS. 20 μL of hydrogel (20 μg of CpG-FITC and PTX in 10 % of RCP solution, respectively) were placed in a test tube and gelated at 37 °C. After formulation of hydrogel, each tube was poured in 2 mL of PBS and then incubated 37 °C under mild shaking motion (50 rpm). The PBS solution was replaced periodically with a fresh PBS and the incubated samples were stored at −80 °C until analysis. The released CpG and PTX were measured *via* fluorescence intensity (Promega, GloMax Discover Plate Reader, Madison, WI, USA) and UV–vis spectrum (Scinco S-3100, Korea) and calculated by an established standard curve.

2.8. Mice and cell lines

The B16F10 and CT26 cell lines were purchased from the American Type Culture Collection (Manassas, VA, USA). NIH3T3 cell line was purchased from the Korean Cell Line Bank (Seoul, Korea). Cancer cell lines were cultured in RPMI1647 containing 10 % fetal bovine serum, 100 units/mL Penicillin G, and 100 μg/mL streptomycin at 37 °C in 5 % CO_2 incubator. C57BL/6 (female, 6-weeks-old) and Balb/c (female, 6-weeks-old) mice were purchased from the Orient Bio (Seongnam, Korea). All experiments with live mice were carried out in compliance with relevant laws and institutional guidelines of the Institutional Animal Care and Use Committee (IACUC) at the Korea Institute of Science and Technology (KIST), and IACUC approved the experiment (approval number: 2021-03-032).

2.9. In vitro culture of BMDMs and BMDCs

Bone marrow-derived macrophages (BMDMs) and Bone marrow-derived dendritic cells (BMDCs) were generated from the bone marrow of C57BL/6 mice (female, 6-weeks-old) [32,33]. Bone marrow cells were flushed from femurs and tibia using RPMI1647 containing 10 % fetal bovine serum, 100 units/mL Penicillin G, and 100 μg/mL streptomycin. Red blood cells were removed by diluted red blood lysis buffer (BioLegend). After cells were incubated at 37 °C for 1 day, non-adherent cells were harvested and seeded at 2×10^6 cells for BMDMs and 5×10^6 cells for BMDCs on 100 mm Petri dishes. The cells were cultured in a medium with M-CSF (20 ng/mL) for BMDMs and GM-CSF

(20 ng/mL) and IL-4 (20 ng/mL) for BMDCs at 37 °C in a humidified atmosphere with 5 % CO_2 to acquire immature phenotypes, respectively. After 7 days, differentiated cells were harvested, washed two or three times with PBS, and used for *in vitro* tests. Differentiated BMDMs and BMDCs were defined as represented subpopulations with the purity displayed as the percentage of the parent population gated on FSC/SSC (Fig. S10).

2.10. Evaluation of in vitro biocompatibility

For evaluation of *in vitro* cytotoxicity, NIH3T3 cells, and BMDMs were seeded in 96-well tissue culture plates at a density of 1×10^4 cells per well. After incubation for 24 h, the cells were washed with PBS. Then, 0.2 mL of the polymer solutions for test samples were added to each well, and the plates were incubated for 24 h at 37 °C in a humidified atmosphere with 5 % CO_2. Cell viability was measured using the 3-(4,5-dimethylthiazol-2-yl)-2,5 diphenyltetrazolium bromide (MTT) and the EZ-CYTOX assay kit (Dogen Bio, Korea) following the manufacturer's instructions. The absorbance was determined at a 570-nm and 450-nm wavelength, respectively, using a microplate reader (Molecular Devices).

2.11. Evaluation of in vivo biocompatibility

For *in vivo* biocompatibility test, 100 μL of the polymer solution (10 wt%) was injected into the dorsal subcutis of 6-week-old female C57BL/6 mice. Blood was collected *via* cardiac puncture and centrifuged at 5000 rpm for 5 min at 4 °C to remove the clot using clot activator gel tubes. Serum clinical chemistry parameters were analyzed with the Beckman AU480 instrument (CA, USA), performed by IDEXX BioAnalytics.

To evaluate the excellent performance of local and sustained release, 10 % hydrogel and diluted RCP polymer solution were prepared. The same dose of PTX (20 μg)and CpG (20 μg) was mixed into the hydrogel and polymer solution. Baseline levels of interleukin-1β (IL-1β), interleukin-12p70 (IL-12p70), interleukin-2 (IL-2) and interferon γ (IFNγ) were determined from peripheral blood before administration. Subcutaneous and intravenous injections were used to administer the RCP hydrogel and diluted solution, respectively, to the mice. Blood samples were collected on days 1, 2, 7, and 14 after administration. Plasma samples were obtained from the blood and used to measure cytokine concentrations using corresponding ELISA Kits according to the vendor's protocols. All blood samples were stored at −20 °C until analysis.

2.12. In vitro receptor-mediated cellular uptake assay

Nile Red (NR, Sigma-Aldrich), a hydrophobic fluorescent dye, was used as a model compound for PTX because its physical properties are very similar. Furthermore, NR can interact with the hydrophobic core part of the polymeric complex *via* a hydrophobic interaction [34]. When 20 μL of the polymer solution was mixed with 1 ng NR and sonicated for 30 min, the mixture formed a nano-sized complex structure. B16F10 cells were seeded in confocal dishes and 96-well plate (2.5×10^4 cells per well) and incubated overnight in a complete RPMI1640 culture medium. To block RGD binding integrin receptor on the cell surface, B16F10 cancer cells were pre-treated with soluble RGD (0.5 mM) at 37 °C for 30 min to block RGD specialized integrin and then washed twice with PBS to remove excess RGD in a medium. Afterward, the culture medium was replaced with a serum-free medium containing NR with or without the polymer. All test samples were incubated at 37 °C for 2 h. After washing with PBS, fluorescence images of the cultured macrophages were captured using a confocal microscope (Olympus). The intensity of Nile Red fluorescence was quantified using a fluorescence spectrophotometer Spectramax M2 (CA, USA).

2.13. In vitro cancer cell death assay

For the *in vitro* assay, 0.01 % hydrogel solution of RCP, RCP-P, RCP-C, RCP-PC (PTX 5 μg/mL, CpG 5 μg/mL), and PBS (as control) was treated in B16F10 tumor cells at 37 °C for 24 h, respectively. Apoptosis was analyzed by a FITC Annexin V Apoptosis Detection Kit with propidium iodine (Invitrogen, V13245), according to the manufacturer's instructions, and a SONY MA900 cell sorter. ICD induced by RCP nanocomplexes was characterized by the release of HMGB1, expression of HSP70, generation of intracellular ROS, and exposure of calreticulin (CRT). B16F10 tumor cells (6-well plates at a density of 1×10^6 cells per well) were cultured for 24 h in FBS-free media, followed by RCP, RCP-P, RCP-C, RCP-PC, and PBS (as control). The presence of HMGB1 in the supernatant was assessed by an ELISA kit (Chondrex Inc.), according to the manufacturer's instructions. The expression of HSP70 was observed by western blotting and GAPDH typically was utilized as a loading control. The generation of intracellular ROS and exposure of CRT were analyzed by staining with DCFH-DA (Abcam) and antibodies for CRT detection (Invitrogen), according to the manufacturer's instructions, and a SONY MA900 cell sorter, respectively. Fluorescence images of CRT exposure were also observed *via* antibody detection with DAPI.

2.14. In vitro activation assay of BMDMs and BMDCs

BMDMs and BMDCs were incubated with the diluted solution of RCP, RCP-P, RCP-C, RCP-PC (PTX 5 μg/mL, CpG 5 μg/mL), and PBS (as control) at 37 °C for 24 h. The culture supernatants were collected, and the levels of secreted INFγ and IL12p70 were analyzed by ELISA (BioLegends, San Diego, CA, USA) according to the manufacturer's instructions. The collected cells were washed and pre-blocked with anti-CD16/32 for 20 min at 4 °C and then labeled with fluorescence-conjugated antibodies as per the manufacturer's protocol (Table S2). The activation level of BMDM and BMDC was quantified by a flow cytometer (MA900, SONY biotechnology, Japan). Inflammatory responses were measured using NF-κB activation (i.e., nuclear translocation of p65). BMDMs and BMDCs were treated with the diluted solution of RCP, RCP-P, RCP-C, RCP-PC, and PBS (as control) at 37 °C for 6 h. A total of 20 μg of protein from BMDM and BMDC extracts were analyzed for immunoblotting and detected using primary antibodies specific for phosphate p65 (p-p65, #3033), p65 (#8242), and GAPDH (#5174), which were purchased from Cell Signaling Technology. Luminescent images were analyzed using iBright Imagers (CL1500, Invtrogen, USA).

2.15. In vivo tumor model

To generate a syngeneic tumor mouse model, 5×10^5 B16F10 and CT26 cells in 100 μL of PBS were subcutaneously injected into the right flank of C57BL/6 and Balb/c mouse, respectively. After 7–8 days, when the volume of tumor reached around 80 mm^3, gels containing RCP (20 mg, hydrogel only), RCP with PTX (20 μg, RCP-P), RCP with CpG (20 μg, RCP-C), or RCP with PTX/CpG (RCP-PC) were intratumorally administrated, respectively. The mice groups were prepared for the analysis of infiltrated immune cells in tumors ($n = 5$ for day 3 and day 7, respectively) and the observation of tumor volume and survival ($n = 6$–8). All mice were randomly divided into 5 groups for each assay.

For combination therapy, B16F10 or CT26 tumor-bearing mice received RCP-PC alone or in combination with an intraperitoneal injection of αPD-1 (100 μg) in PBS according to a predefined schedule. To verify the systemic immune response, 3×10^5 B16F10 cells were inoculated into the opposite side of the flank at the days of hydrogel injection. The tumor volume and body weight of mice were quantified every other day. The tumor volume was measured using electronic calipers and calculated using the formula: tumor volume = length × width × height × 1/2. Mice were sacrificed when the volume reached 1000 mm^3 in the B16F10 and CT26 models.

2.16. Analysis of infiltrating immune cells in tumor

To analyze the infiltrating immune cells after treatment, the tumors, tumor-draining lymph nodes (TDLNs), and spleen were isolated after sacrifices. The tumors and TDLNs were chopped into small pieces and resuspended in Gentle Collagenase/Hyaluronidase (Stemcell Technologies) diluted in RPMI1640. The solutions were incubated for 1 h at 37 °C. The spleen tissue samples were dissociated mechanically. The cells from the tumor, TDLNs, and spleen were washed twice with PBS and lysed with a diluent red blood lysis buffer. After centrifugation, the cells were filtered through a cell strainer, centrifuged, and resuspended. To block non-specific staining, obtained single-cell suspensions were pre-blocked with anti-CD16/32 for 20 min at 4 °C and then were labeled with fluorescence-conjugated antibodies as per the manufacturer's protocol (Table S2). For intracellular staining, suspended cells were simultaneously fixed and permeabilized by BD Cytofix/Cytoperm. Fluorescence-activated cell sorting analyses were collected in MA900 (SONY biotechnology, Japan) and analyzed using FlowJo v5.0 (Tree Star, Ashland, OR, USA) software.

2.17. In vivo PTX and CpG retention test

The 5×10^5 cells of B16F10 in 100 μL of PBS were injected into the right dorsal subcutis of C57BL/6 mice (5 weeks, female, from the Orient Bio, Korea). When the mean volume of tumors reached approximately 80 mm^3, the RCP solution mixed with Nile Red (20 μL) or FITC tagged CpG (20 μL) was injected intratumorally. The intensity of Nile Red or FITC was checked at predetermined schedules by the IVIS platform (In Vivo Imaging System, Caliper Life Sciences Inc., Hopkinton, MA, USA).

2.18. Statistical analysis

Data was presented as the mean with standard deviation (SD) or standard error of the mean (SEM). Statistical analysis was performed using GraphPad Prism software (version 5.0, Graph Pad Software Inc., La Jolla, CA). For statistical analysis, comparisons between groups were performed with one-way ANOVA followed by Tukey's post-hoc test. Repeated-measures two-way ANOVA was used to compare differences in the tumor growth curve by post hoc Bonferroni analysis. Animal survival was plotted using Kaplan-Meier curves and its multiple comparisons were assessed using log-rank (Mantel-Cox) tests. * **, ***, and ns indicate $P < 0.05$, $P < 0.01$, $P < 0.001$ and not significant, respectively. A P-value < 0.05 was considered statistically significant. *In vitro* data using bone marrow cells were collected from separate culture wells derived from a single mouse. The numbers of animals included in the study are noted in each figure legend.

3. Results and discussion

3.1. Synthesis and characterization of the RCP hydrogel

The RCP was synthesized following the reaction scheme depicted in Fig. S1. In brief, we synthesized methacrylated poly (organophosphazenes) (Polymer 1 in Fig. S1), which was substituted with hydrophobic $_L$-isoleucine ethyl ester (IleOEt) and hydrophilic α-amino-ω-methoxy-poly (ethylene glycol) (AMPEG) for sol-gel transition behavior *via* temperature-dependent hydrophobic interaction changes [35]. 2-aminoethyl methacrylate (2-AM) in Polymer 1 provides the terminal methacrylate group which can be used to conjugate RC peptide for various functions. The RC peptide design comprised four compartments: 1) tripeptide RGD for the enhanced intracellular delivery of drugs effectively through integrin-mediated endocytosis, 2) oligo glycine (4G) as a spacer for reduced steric hindrance, 3) oligo histidine-arginine (6H4R) for loading anionic adjuvants (e.g., CpG and poly I:C) *via* ionic interaction, and 4) cysteine for conjugation with Polymer 1 (Fig. S2). The RCP was synthesized by the conjugation of the RC peptide to Polymer 1 by thiol–ene crosslinking between the thiol group of the RC peptide and the methacrylate group of Polymer 1. Conjugation of the RC peptide to Polymer 1 was confirmed by ^{1}H NMR spectroscopy (Fig. S3). The ratio of RC peptide conjugation to Polymer 1 was determined by analyzing the peak corresponding to the methacrylate moieties.

3.2. Characterizations of the RCP-based NGN system

The RCP is amphiphilic which results in the formation of nano-sized complexes through hydrophobic interactions mediated self-assembly, primarily involving the IleOEt moiety of the polymer in aqueous environments [36,37]. Furthermore, the hydrophilic and cationic RC peptide within the RCP tends to reside on the surface of these nanocomplexes, establishing direct interactions with water molecules. The surface charge of RCP nanocomplexes measures approximately $+11.6 \pm 0.4$ mV. Consequently, the RCP polymer solution efficiently accommodates both PTX and CpG through hydrophobic and ionic interactions, respectively. The RCP solution containing drugs exhibits a temperature-dependent sol-gel transition phenomenon, which results in the solution changing to hydrogel and existing in a dispersed state within tumor tissue. Subsequently, the hydrogel gradually degrades while encapsulating the drugs in the form of polymeric nanocomplexes for the long term. These nanocomplexes would play a pivotal role in facilitating localized drug delivery within the tumor microenvironment. Accordingly, to explain the three steps of phase transition of RCP, we suggest its phenomenon in terms of 'nano-gel-nano (NGN)', is suitable for this study (Fig. 2A).

First of all, we evaluated the propensity of the RCP to form nanocomplexes with CpG and PTX by gel retardation test and DLS measurement. These cationic polymeric complexes were anticipated to engage in ionic interactions with CpG, a gene-like molecule, to facilitate cellular uptake. The formation of nanocomplexes between CpG and the RCP was observed over 100:1 (RCP: CpG, w/w) without naked CpG (Fig. 2B) in the gel retardation test, and the ratio was fixed for further study. We also postulated that the RCP polymer possesses the capability to establish nanocomplexes with PTX *via* hydrophobic interactions, primarily involving the IleOEt moieties residing within the core of RCP nanocomplexes. Notably, PTX, a poorly soluble chemical drug for anticancers, showed soluble in the RCP polymeric solution until 2 mg/mL (Fig. 2C) which has also confirmed the nano-sized complexity between PTX and the RCP. It was further substantiated by the existence of nano-sized complexes between PTX and RCP, as ascertained through dynamic light scattering (DLS). We confirmed the interaction between the RCP and hydrophobic PTX until 2 mg/ml to construct nanocomplexes (Fig. S4).

In light of the obtained findings, we chose 1 mg/mL of PTX and CpG in 10 % RCP solution, respectively for further study and confirmed the ability of the nanocomplexes formation between RCP, PTX, and CpG. The sizes of the nanocomplexes with drugs were smaller than those of RCP because the compact self-assembled particle formation *via* both hydrophobic and ionic interactions between RCP and PTX/CpG (Fig. 2D). The properties of these nanocomplexes are consistent with those reported previously. These nanocomplexes, approximately 100 nm in size and with a slightly positive surface charge, have the advantage of effective intracellular drug reagent uptake [36,38].

The polymer solution began to increase in viscosity at 28.8 °C and transformed to the hydrogel. The viscosity of hydrogel was shown approximately 300 Pa·s at 37 °C (Fig. 2E) and rheology results also exhibit that the loss modulus (G″) was higher than the storage modulus (G′) at 4 °C whereas G' value was greater than G" at 37 °C (Fig. 2F). This means that the RCP hydrogel exhibited a temperature-dependent gelation profile. Furthermore, the property of thermal gelation is maintained after mixing with PTX/CpG (Fig. S5). As mentioned above, we postulate that the multi-drug-loaded RCP hydrogels were located in the center of the tumor and released the nanocomplexes *via* decomposition for an extended period. The *in vitro* release profile of CpG from RCP hydrogel

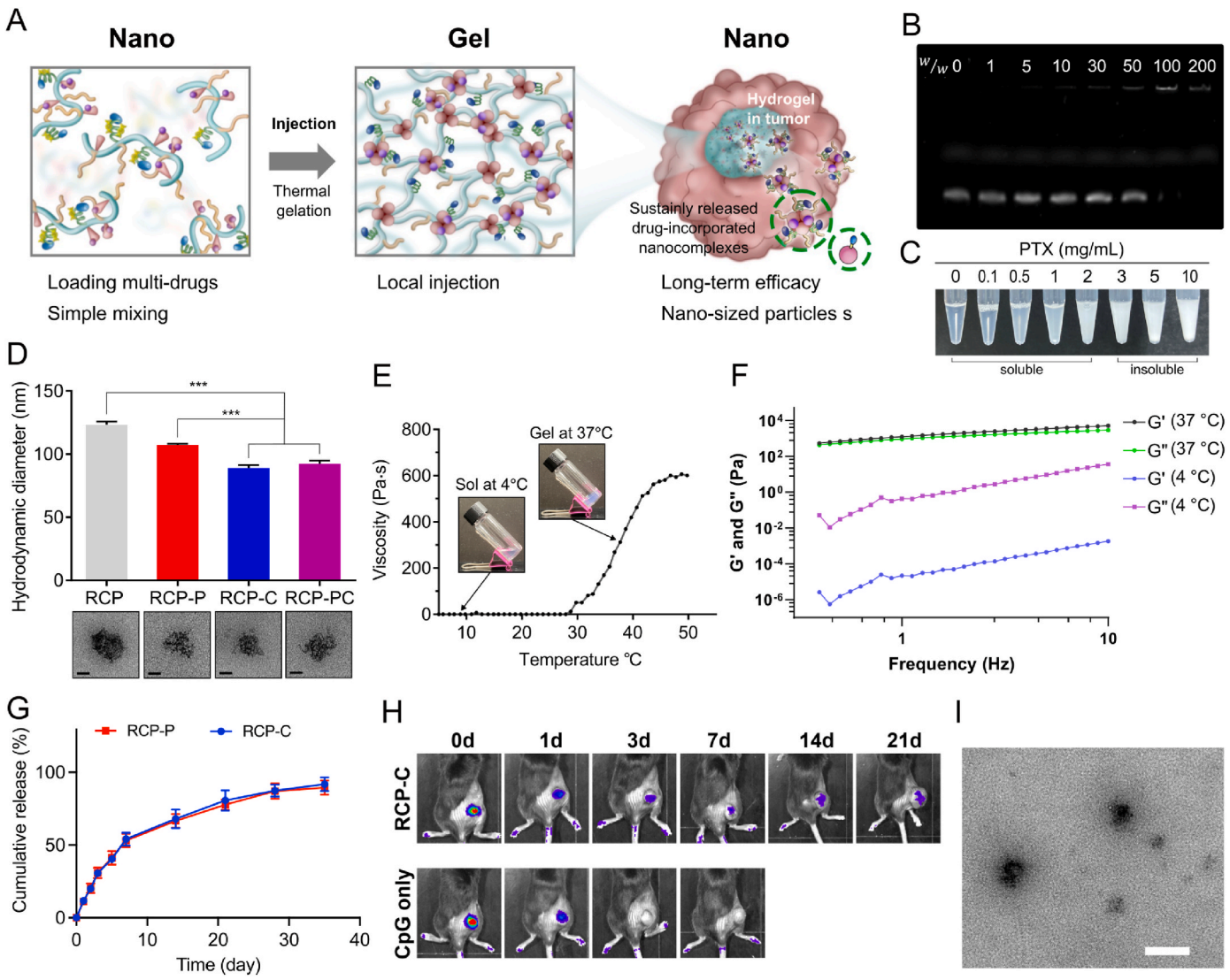

Fig. 2. Characterizations of the RCP hydrogel-based NGN system A) Illustration of concept of nano-gel-nano (NGN) system. B) Gel retardation assay of the RCP/CpG complexes as a function of w/w ratios. C) The photo images of PTX solubility in RCP solution in wide range of concentration. D) Sizes and morphologies of the nanocomplexes (RCP, RCP-P, RCP-C, and RCP-PC; n = 3). Scale bar is 50 nm *** indicates $P < 0.001$ by one-way ANOVA followed by Tukey's post hoc analysis. E) Temperature-dependent sol-gel transition of 10 wt% aqueous RCP solutions. F) The storage modulus (G′) and loss modulus (G″) of the RCP at 4 and 37 °C. G) *In vitro* release profile of dissociated nanocomplexes from the RCP-P and RCP-C hydrogel using PTX and FITC-tagged CpG, respectively. H) IVIS images showing CpG retention within the RCP-C hydrogel of 10 % and CpG alone using FITC-tagged CpG in a B16F10 tumor-bearing mouse. I) Transmission electron microscope (TEM) image of dissociated nanocomplexes from the PCP-PC hydrogel after 7 days of incubation at 37 °C. The scale bar is 200 nm *** indicate $P < 0.001$ by one-way ANOVA followed by Tukey's post hoc analysis.

was estimated using FITC-tagged CpG, PTX allowing for quantification of fluorescence intensity and UV/Vis spectroscopic analysis, respectively. (Fig. 2G). RCP hydrogel showed sustained release of both PTX and CpG. The release patterns of CpG and PTX were almost similar for 35 days. It means both CpG and PTX were released from hydrogel in the form of polymeric complexes with RCP, not in naked forms, individually. To prove the sustained release pattern of the nanocomplexes from the RCP hydrogel in tumor tissues, we investigated the intratumoral retention time of CpG and PTX in the hydrogel using FITC-tagged CpG and Nile Red (NR, as a model for PTX) in tumor-bearing mice. The fluorescence intensity of FITC-tagged CpG in the CpG-only group, which was located in the center of the tumor, decreased instantly and disappeared after 1 day. In contrast, the RCP hydrogel held FITC-tagged CpG, and the fluorescence intensity was maintained for 21 days at the intratumoral injection sites (Fig. 2H). We also confirmed that the intensity of NR in the released nanocomplexes from hydrogel, which was located within the tumor tissue, was maintained for 14 days (Fig. S6). In addition, the nanocomplexes released from the RCP-PC hydrogel showed a 90–100 nm diameter of spherical structure after incubation for 7 days (Fig. 2I). These properties of the nanocomplexes are consistent with those reported previously [36,37,39–41]. These results indicate that the RCP hydrogel can load PTX and CpG by complex formation *via* hydrophobic and ionic interactions, respectively, exhibiting thermo-sensitive sol-gel transitions, and releasing nano-sized polymeric complexes with PTX and CpG for an extended period.

3.3. *In vitro* selective PTX delivery into cancer cells

We postulated that intratumorally injected the RCP hydrogels exhibit sustained release of nano-sized polymeric complexes that can deliver drugs to various cells in the tumor tissue. Prior to the *in vitro* test, we confirmed that the viability of the cultured cells was not affected by the RCP hydrogel solution at a wide range of concentrations (Fig. S7). To achieve a more effective intracellular uptake of the RCP nanocomplexes

into cancer cells, MeAcPPZ was conjugated with an RGD-ended cationic peptide. As previously reported, the RGD moiety can effectively enhance selective binding or penetration of drugs to tumor cells by recognizing integrins, such as $\alpha v\beta 3$, $\alpha v\beta 5$, and $\alpha 5\beta 1$, which are overexpressed in tumor endothelial cells [16,42]. Therefore, it was assumed that the RCP nanocomplexes can dominantly recognize cancer cells among the various types of cells in tumor tissue *via* the RGD moiety, which can elicit receptor-mediated endocytosis and preferentially elicit cell death in cancer cells, compared to other cells in TIMEs (Fig. 3A). We tested whether the RCP nanocomplexes facilitate the cellular uptake of drugs into B16F10 cancer cells by overexpressing RGD-specialized integrins. To visualize the uptake of the nanocomplexes into B16F10 cells *in vitro*, the RCP solutions were mixed with the hydrophobic fluorescent dye NR, a model of PTX that can interact with the hydrophobic core of the polymeric complex *via* hydrophobic interactions [34,43]. When the RCP polymer solution was mixed with NR (0.5 μg/mL), the mixture formed a nano-sized complex structure with no significant difference in size between the RCP-P and RCP-NR (Fig. S8). We expected that if the nanocomplexes facilitated intracellular uptake into cancer cells, NR dye in the nanoparticles would localize within the intracellular region. The red fluorescence in B16F10 cancer cells was markedly higher when treated with the RCP-NR than when treated with NR in DMSO. Furthermore, the fluorescence intensity of cancer cells was reduced after pretreatment with soluble RGD, suggesting that intracellular uptake through RGD-related receptor-mediated endocytosis is dominant compared to passive endocytosis (Fig. 3B and C). This suggests that the nanocomplexes have the chance to deliver cancer cells preferentially among various cell types in complex TIMEs.

3.4. *In vitro cancer cell death via intracellular uptake of the nanocomplexes*

Since it was confirmed that cellular uptake of the RCP nanocomplexes into cancer cells was enhanced by the interaction of RGD and integrin, we next analyzed the pattern of cancer cell death induced by the nanocomplexes. We chose PTX as the chemotherapeutic agent to induce ICD in tumor cells, which could stimulate immunogenic responses by the release of TAAs as well as damage-associated molecular patterns (DAMPs) [44–46]. Apoptotic cancer cell death was assessed by flow cytometry analysis using Annexin V and propidium iodide staining (Fig. 3D and Fig. S9). As expected, the RCP-P and RCP-PC groups showed significantly higher PTX-mediated apoptotic cell death rates than the other groups. It has been reported that ICD is accompanied by the generation of reactive oxygen species (ROS) [47], resulting in the expression of DAMPs [44], which are characterized by the release of high mobility group box 1 (HMGB1) [48], expression of heat-shock protein 70 (HSP70) [49], and exposure of calreticulin (CRT) [50,51] on the cell surface. As shown in Fig. 3E, B16F10 cells undergoing ICD apoptosis generated intracellular ROS in the RCP-P and RCP-PC groups. We also observed that in both the RCP-P and RCP-PC groups, the secretion of HMGB1 and the expression of HSP70 in B16F10 cells were remarkably increased (Fig. 3F and G). CRT exposure on the cell surface was monitored using confocal microscopy and flow cytometry (Fig. 3H and I). These DAMP markers serve as an activation of the “eat me” signal to APCs (such as macrophages and DCs), which can induce immunogenic uptake of TAAs [50].

We confirmed the slowly degradable released nanocomplexes from hydrogel were incorporated with PTX and CpG (Fig. 2I), and then assessed the maintenance of drug efficacy within nanocomplexes. The sustained released nanocomplexes showed inhibition of cancer cell growth compared to the control group but similar to fresh formulation with the same concentration of PTX (Fig. 3J). It indicates that the nanocomplexes can conserve their drug efficacy in the long term. Based on the results above, we confirmed that the RCP-PC nanocomplexes could be preferentially delivered into integrin-overexpressing cancer cells by RGD-receptor-mediated endocytosis, followed by induction of apoptotic cancer cell death. These results suggested that the RCP-based NGN system can generate not only DAMPs but also TAAs in local TIMEs effectively, resulting in inducing immune responses while reducing systemic side effects for an extended period.

3.5. *In vitro immunostimulatory activity of the nanocomplexes*

Although the release of TAAs and DAMP signals with PTX can also modulate the immune response in the TIME, we chose cytosine-phosphodiester guanine oligonucleotides (CpG), which are TLR9 agonists, as adjuvants to promote further immune activation (Fig. 4A). To investigate the effect of the nanocomplexes on immune cell activity, bone marrow-derived macrophages (BMDMs) and bone marrow-derived dendritic cells (BMDCs) were cultured from bone marrow monocytes.

First, to investigate whether immune cells were affected by the RCP hydrogel, we tested *in vitro* cytotoxicity using BMDMs and confirmed that the RCP hydrogel did not exhibit significant cytotoxicity with BMDMs at a wide range of concentrations (Fig. S11AA). Although apoptotic cell death of B16F10 tumor cells was induced by the RCP-P and RCP-PC, these formulations did not show any significant toxicity toward BMDMs at similar concentrations (Fig. S11B). Moreover, BMDMs in RCP-C showed increased proliferation in the MTT assay, indicating that BMDMs were stimulated by CpG (Fig. S11A). This suggests that cellular uptake of CpG could induce mitochondrial remodeling in immune cells, resulting in the activation and production of cytokines, chemokines, and even metabolites to stimulate effective immune responses [52]. Cellular uptake of the RCP complexes containing FITC-tagged CpG in BMDM and BMDC was observed to determine whether the nanocomplexes are advantageous for drug delivery to immune cells. Similar to uptake into cancer cells, RCP with CpG showed higher fluorescence intensity in BMDMs and BMDCs than naked CpG (Fig. 4B). It means that the RCP nanocomplexes with CpG can facilitate cellular uptake in the form of nanocomplexes. We next examined whether the nanocomplexes could induce the maturation or activation of APCs. The activation or maturation of APCs is regulated through the nuclear factor κ-light chain of enhancer-activated B cells (NF-κB) pathway, which plays a pivotal role in the regulation of genes involved in pro-inflammatory cytokines and induction of antigen-specific T cell responses [53,54].

Therefore, we assessed the expression of inflammatory transcription factors and the secretion of pro-inflammatory cytokines from BMDCs and BMDMs by the nanocomplexes (Fig. 4C–G and Fig. S12A-E). p65, a member of the NF-κB transcription factor family, is involved in the production of pro-inflammatory cytokines, and is primarily localized to the cytoplasm in an inactive state (p65) and translocated into the nucleus upon activation (p-p65) [53]. After incubation with the nanocomplexes, the expression of p-p65 and the secretion of pro-inflammatory cytokines (IL-6, IL-12p70, IFNγ, and TNFα) in BMDCs (Fig. 4D–G) after treatment with the RCP-P, RCP-C, and RCP-PC nanocomplexes were notably higher than those in the control and the RCP groups. The expression of CD40 and major histocompatibility complex class *II* (MHC*II*) from BMDCs was increased in the RCP-P and RCP-PC, which can induce immunostimulatory activity in DCs (Fig. 4H and I), possessing the ability to present antigens to T cells [53,55]. In addition to BMDCs, the RCP-PC nanocomplexes also modulate macrophages (BMDMs) as shown in Fig. S12. Tumor-associated macrophages (TAMs) are one of the most amount of infiltrated cells in tumor tissues that elicit immunosuppressive factors. Thus, re-polarizing the immune-suppressed and anti-inflammatory phenotype of macrophages (M2) to pro-inflammatory phenotype for enhancing immune-mediated therapeutic efficacy [56,57]. While the RCP-P nanocomplexes-treated BMDMs exhibited minute NF-κB transcription factor activity, the expression of p-p65 in BMDCs was increased by PTX (Fig. S12). This suggests that PTX is generally known to act as an ICD inducer, but it has recently been reported to act as a TLR4 agonist that can suppress the induction of M2 macrophages and enhance the maturation of DCs [58].

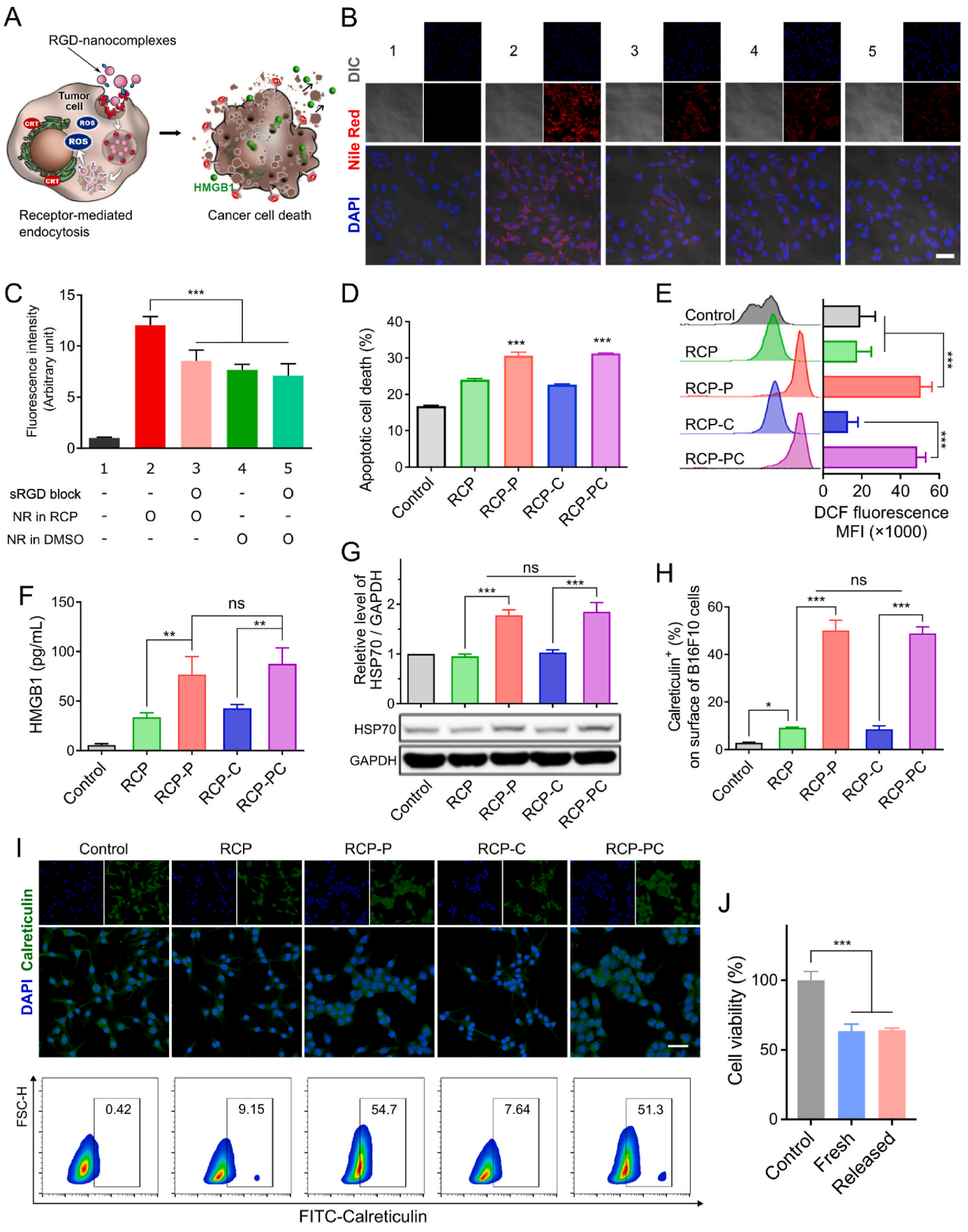

(caption on next page)

Fig. 3. ***In vitro*** **selective PTX delivery-mediated cancer cell death for TAA release** A) Schematic illustration of active intracellular uptake of the nanocomplexes into cancer cells through RGD moiety and release of DAMPS by immunogenic cell death. B) Representative images of RGD moiety-dependent cellular uptake of the RCP nanocomplexes with Nile Red (NR) in B16F10 cancer cells. The scale bar represents 50 μm. C) Quantification of NR fluorescence intensity (n = 5). D) Percentages of apoptosis in B16F10 cells (Annexin-V positive cells: early and late apoptosis stage) after treatment of the nanocomplexes (RCP, RCP-P, RCP-C, RCP-PC; PTX 5 μg/mL, CpG 5 μg/mL). E) Flow cytometry for the quantification of intracellular ROS level using DCFH-DA 24 h following treatment. F) Quantification of HMGB1 in supernatant of B16F10 cells by ELISA 24 h following treatment. G) Western blot assay of the HSP70 expression in B16F10 cells after 24 h of treatment. The graph under the western bands shows the relative protein expression of HSP70 by quantifying the greyscale values with ImageJ. H) Quantification of calreticulin expression on the cell surface by flow cytometry analysis 24 h following treatment. I) Immunofluorescence images and dot plots of CRT expression on the B16F10 cells after 24 h with different treatments. J) Cell viability for checking the reducing cancer cell growth in the B16F10 cell line by PTX that was released from 10 % RCP-PC hydrogel after 7 days at 37 °C. * **, ***, and ns indicate $P < 0.05$, $P < 0.01$, $P < 0.001$ and not significant, respectively by one-way ANOVA followed by Tukey's post hoc analysis.

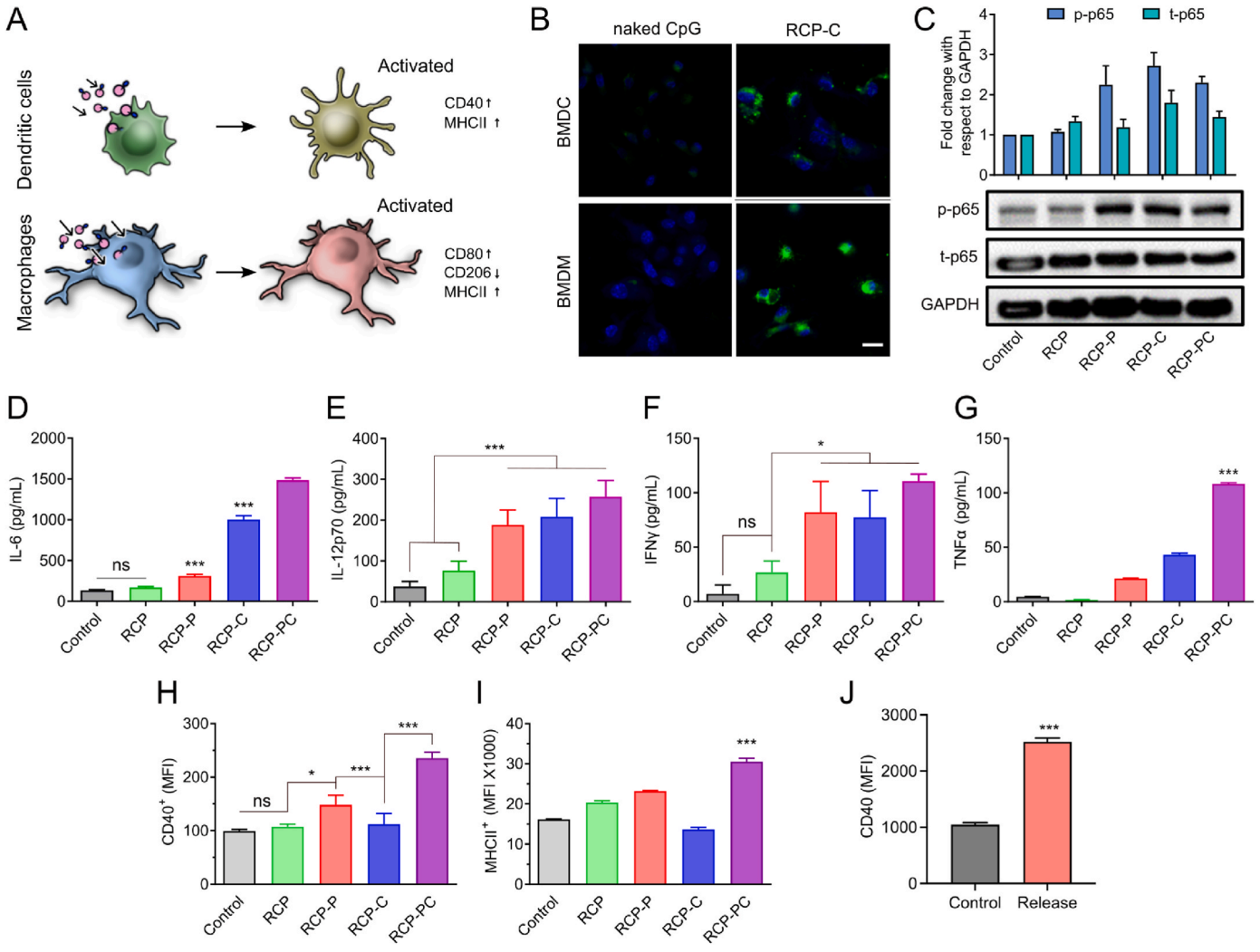

Fig. 4. ***In vitro*** **selective adjuvant delivery-mediated immune modulation of BMDCs.** A) Schematic illustration of activation of APCs by the nanocomplexes. B) Confocal images of *in vitro* cellular uptake of the RCP nanocomplexes with FITC tagged CpG in BMDM and BMDC after 2 h. Scale bar represents 20 μm. C) Western blot assay of the NF-κB (total p65 and phosphate p65) expressions in BMDCs. Cytokine levels of D) IL-6, E) IL-12p70, F) IFNγ, and G) TNFα in supernatant of BMDCs measured by ELISA (n = 3 from different culture wells). Flow cytometry for the surface markers of H) CD40 and I) MHC*II* expression in BMDCs (MFI, mean fluorescence intensity) J) CD40 expression in BMDCs by the RCP-PC nanocompelxes that was released from 10 % RCP-PC hydrogel after 7 days at 37 °C. All results were obtained from three different culture wells (n = 3). * **, ***, and ns indicate $P < 0.05$, $P < 0.01$, $P < 0.001$ and not significant, respectively by one-way ANOVA followed by Tukey's post hoc analysis.

Similar to BMDCs, the treatment of the RCP-PC group showed highest the secretion of pro-inflammatory cytokines (IL-6, IL-12p70, and IFNγ) in BMDMs compared to others (Fig. S12B-E). The expression of CD80 and MHC*II* in BMDMs, the M1 macrophage markers, were increased, while the expression of CD206 as M2 marker was decreased by the RCP-C and RCP-PC (Fig. S12F-H). These indicated that the RCP-PC could induce the polarization of macrophages in tumor to immunogenic types. Interestingly, the moderate secretion of pro-inflammatory cytokines in the RCP-P, RCP-C, and RCP-PC groups showed synergistic secretion in both BMDCs and BMDMs. This indicates that the RCP-PC nanocomplexes can be used as effective adjuvants in cancer vaccines to induce enhanced APC activation, which elicits the initiation of the immune response between APCs and T cells [59].

We also assessed the nanocomplexes efficacy for the long term using the same samples in Fig. 3J. As the similar pattern of Fig. 4H, the expression of CD40 on BMDCs was increased compared to the control

group (non-treated), suggesting that the polymeric nanocomplexes protect the PTX/CpG and maintain their efficacy for the long term (Fig. 4J).

3.6. Orchestration of anti-tumor immune responses by the RCP-PC hydrogel system

Before checking the anti-tumor effects of the RCP-PC hydrogel system hydrogel, we confirmed the safety of the injected RCP hydrogel as a carrier material by monitoring the serum levels of biomarkers and body weight changes. Compared with the control group (saline injection), the RCP hydrogel showed no liver and kidney toxicity, with no significant body weight difference over 5 days (Table S1).

The anti-tumor effect of the RCP-PC hydrogel system was evaluated in a B16F10 tumor model (C57BL/6, female, 6-week-old). When the tumor reached a volume of approximately 80 mm^3, the tumor-bearing mice were randomly divided and treated with (1) PBS as a control (n = 6), (2) RCP (n = 8), (3) RCP-P (n = 8), (4) RCP-C (n = 8), and (5) RCP-PC (n = 8) *via* single intratumoral administration. Tumor volumes and survival patterns of all groups were monitored for 40 days (Fig. 5A). While the RCP-P and RCP-C moderately inhibited tumor growth, the RCP-PC group significantly inhibited tumor growth, resulting in prolonged survival and complete cure in 25 % of mice (Fig. 5B–E). This suggests that the combination of ICD inducer (PTX) and adjuvant CpG in RCP-PC hydrogel treatment provided a synergistic therapeutic effect. We investigated the immunological mechanisms of the antitumor effects

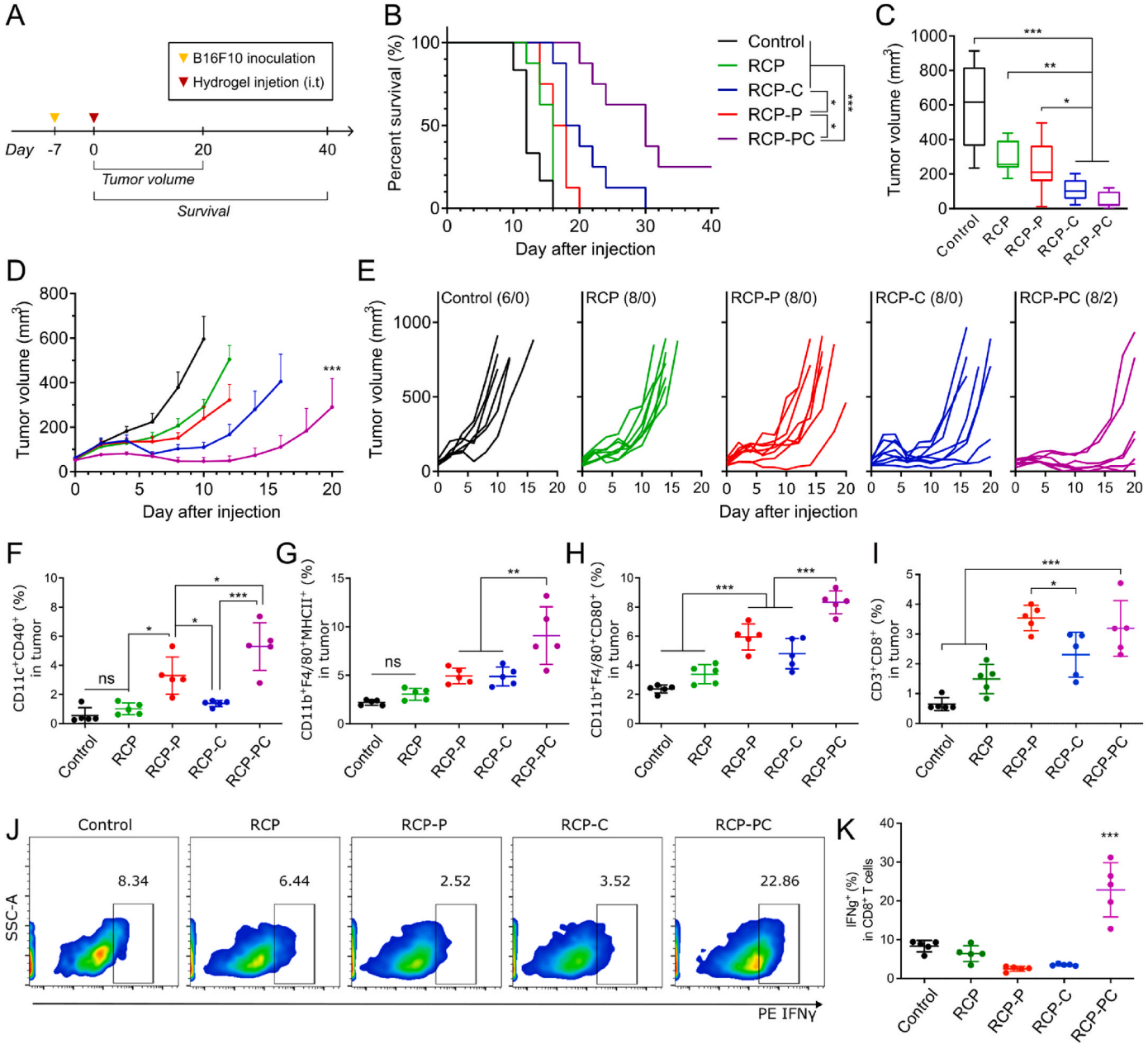

Fig. 5. Antitumor effects with TIME modulation. A) Schematic illustration of schedule for *in vivo* study. B) Survival rates as determined by Kaplan–Meier analysis (n = 6–8). C) Tumor volumes on day 10. D) Tumor volume changes until day 20. E) Individual tumor volumes until day 20. Numbers on the top side represent the number of tumor-free mice and median survival (m.s.). F) Percentages of $CD40^+$ DCs in tumor on day 3 (n = 5). G) Percentages of $CD80^+$ and H) $MHCII^+$ macrophages in tumor on day 3 (n = 5). I) Percentages of $CD8^+$ T cells in tumor day 7 (n = 5). J) Representative dot plots for $IFN\gamma^+$ on $CD8^+$ T cells; K) Percentages of $IFN\gamma^+$ on $CD8^+$ T cells in tumor (n = 5). * **, ***, and ns indicate $P < 0.05$, $P < 0.01$, $P < 0.001$, and not significant, respectively by one-way ANOVA followed by Tukey's post hoc analysis.

of RCP hydrogel systems to prove the *in vivo* results was due to the multiple targetability-mediated generating TAAs and DAMPs as well as activating APCs. Tumor-infiltrating lymphocytes (TILs) from the remaining tumor tissues were analyzed by flow cytometry on days 3 and 7 after the intratumoral injection (Fig. 5F–K, gating strategy shown in Fig. S13). The population of infiltrated immune cells ($CD45^+$) in the tumors was higher in the RCP-P and RCP-PC groups than in the other groups (Fig. S14). It was assumed that the preferential cellular uptake of PTX into cancer cells in the TIME might begin to evoke immune reactions. We observed infiltration of DCs and macrophages into the tumor sites on day 3. The RCP-PC group showed significantly increased expression levels of costimulatory molecules (CD40) on $CD45^+$ $CD11c^+$ DCs from the tumor sites (Fig. 5F). Activated ($CD80^+$, $MHCII^+$; M1 like) TAMs were also elevated in the RCP-PC group (Fig. 5G and H).

Activated macrophages and mature DCs, stimulated by both ICD induction and TLR activity, play a pivotal role in antigen-specific T cell immunity. The number of infiltrating effective T cells in the TIME typically indicates the intensity of the immunogenic therapeutic response [60,61]. Therefore, we investigated T cell populations in the TIME on day 7. As shown in Fig. 5I, the infiltration of $CD3^+$ and $CD8^+$ cells significantly increased in the RCP-P and RCP-PC groups. However, the number of $CD3^+$ $CD8^+$ $IFN\gamma^+$ T cells markedly increased in the RCP-PC group, which led to the orchestration of innate and adaptive immune responses through the combination of immunogenic cancer cell death by PTX and the activation of immune cells by CpG (Fig. 5J and K). During the *in vivo* experiment, the body weights of all groups showed no significant change, indicating no severe acute systemic toxicity (Fig. S15).

3.7. Evaluation of immunotherapeutic efficacy and toxicity in different administration types of the nanocomplexes

Driven by the superior therapeutic efficacy of the RCP-PC in the tumor model, we tried to investigate whether sustained drug delivery could show therapeutic effects as well as minimal systemic side effects. To verify the efficacy of the sustained released nanocomplex system, we prepared mice bearing B16F10 tumors and randomly divided them into three groups (n = 5), as shown in Fig. 6A. The RCP-P gel group showed inhibited tumor growth and prolonged survival compared to the PBS and RCP-P solution groups (Fig. 6B and C).

Next, we further monitored the changes of pro-inflammatory cytokines in mouse peripheral blood after local and systemic administrations as shown in Fig. 6D. Thus, assessing cytokine storm effects on the local sustained released drug system compared to systemic nanoparticle-based drug delivery system. The dose of PTX and CpG were 20 μg/mL respectively with 200 μg/mL of RCP per mouse. The concentrations of pro-inflammatory cytokines (IL-1β, IL-12p70, IL-2, and INFγ) which are related to cytokine storm, were assessed using ELISA [62]. There was no significant difference in the amount of pro-inflammatory cytokines among the groups at day 0. Both subcutaneous (s.c.) single injection of the RCP-PC and intravenous (i.v) injections of the RCP groups showed no obvious increases in the concentrations of these four pro-inflammatory cytokines, but i.v injection of the RCP-PC group showed a dramatic increase at day 1 and 2. This indicates that the RCP can be used as a safe material for immunotherapy, providing sustained release of drugs at local sites and inhibiting cytokine storm effects. The injectable hydrogel can achieve high local bioactive drug concentrations to reduce systemic side effects, as well as sustained supplementation of therapeutic drugs. These results suggest that the delivery pattern *via* sustained release from the hydrogel may play an important role in inducing effective immunogenic anticancer efficacy with minimally systemic toxicity.

3.8. Therapeutic effects of the RCP-PC treatment in enhancing anti-tumor immune response to checkpoint inhibitors and inducing the systemic immunity

Considering the increased number of effective T cells ($CD8^+$ $IFN\gamma^+$) in TIME after intratumoral administration of the RCP-PC, we hypothesized that the TIME reprogrammed by the action of the hydrogel-based *in situ* cancer vaccine could elicit enhanced ICB therapeutic response [8,9]. B16-F10 tumor-bearing mice (C57BL/6, female, 6-week-old) were prepared and randomly divided into four groups: (1) PBS as a control (n = 8), (2) αPD-1 (n = 8), (3) RCP-PC (n = 8), and (4) RCP-PC with αPD-1 (n = 8). PBS and hydrogel were administered *via* intratumoral injection once, and αPD-1 was intraperitoneally injected three times at 2-day intervals. Tumor volumes and survival patterns of all groups were monitored for 40 days (Fig. 7A). In the B16F10 model, the RCP-PC with αPD-1 substantially inhibited tumor growth and improved survival rates compared to those in the single treatment groups (Fig. 7B and C, Fig. S16). The median survival (m.s.) of mice treated with the RCP-PC with αPD-1 was 34 days, while the m.s. of mice with a single treatment of αPD-1 and the RCP-PC were 22 and 18 days, respectively. In addition to melanoma, the RCP-PC combined with αPD-1 was also effective in the colon cancer (CT26) model (Balb/c, female, 6-weeks-old), as shown in Fig. S17. The pattern of therapeutic and synergistic effects with αPD-1 were similar to those observed in the B16F10 model. These results indicate that intratumoral injection of the RCP-PC induced an immunogenic TIME by the generation of *in situ* tumor antigens and the modulation of immunosuppressive cells, resulting not only in the induction of an effective T cell-mediated immune response but also in an enhancement of the effect of immune checkpoint inhibitors. This injectable *in situ* cancer vaccine platform based on hydrogel can be applied to various types of solid tumors.

Recent studies have shown that local immunogenic responses in primary tumors can elicit systemic therapeutic effects on distant tumors [63,64]. We also investigated the long-term potent memory response lasting for the long term by performing a tumor rechallenge test. The surviving mice that were cured of tumors in the RCP-PC with αPD-1 treatment group (as shown in Fig. 7A–C) were the focus of our attention. They were reinoculated with B16F10 cells on the flank opposite the primary tumor site 60 days after the final treatment. While naïve mice developed tumor growth, the rechallenged tumor growth in the cured mice was inhibited for up to 15 days (Fig. 7D). The results confirmed that the *in situ* RCP hydrogel vaccine induced long-lasting antitumor immunity by inducing memory T cell responses.

To investigate whether the systemic antitumor immune response could be induced by a combination of intratumoral injected RCP-PC hydrogel and ICB (αPD-1), mice bearing B16F10 tumors were randomly divided into three groups: (1) PBS as a control (n = 8), (2) RCP-PC (n = 8), and (3) RCP-PC with αPD-1 (n = 8). After hydrogel injection, we inoculated the mice with cells for secondary tumor formation contralaterally to the primary tumor (Fig. 7E). It was assumed that the growth of secondary tumors would be retarded by increased memory T cells, which could induce a systemic (abscopal) responses. The growth of the primary tumor was significantly inhibited by the groups of RCP-PC and RCP-PC with αPD-1. Moreover, the number of surviving mice and inhibition of secondary tumor development were also higher than those in the control group (Fig. 7F and G). To investigate the effect of the RCP-PC treatment on the systemic memory T cell response *in vivo*, we isolated T cells from tumor-draining lymph nodes (TDLNs) and spleens of surviving mice 19 days after intratumoral injection and analyzed their populations by flow cytometry. $CD3^+CD8^+CD44^+$ cells were considered memory T cells [65,66]. The gating strategy is illustrated in Fig. S18. Compared with naïve mice (control group), the population of infiltrated $CD8^+$ T cells, memory T cells in TDLNs and spleens were remarkably increased in the RCP-PC and RCP-PC with αPD-1 (Fig. 7H–J and Fig. S19). These results suggest that the therapeutic efficacy of the RCP-PC with αPD-1 induces long-lasting

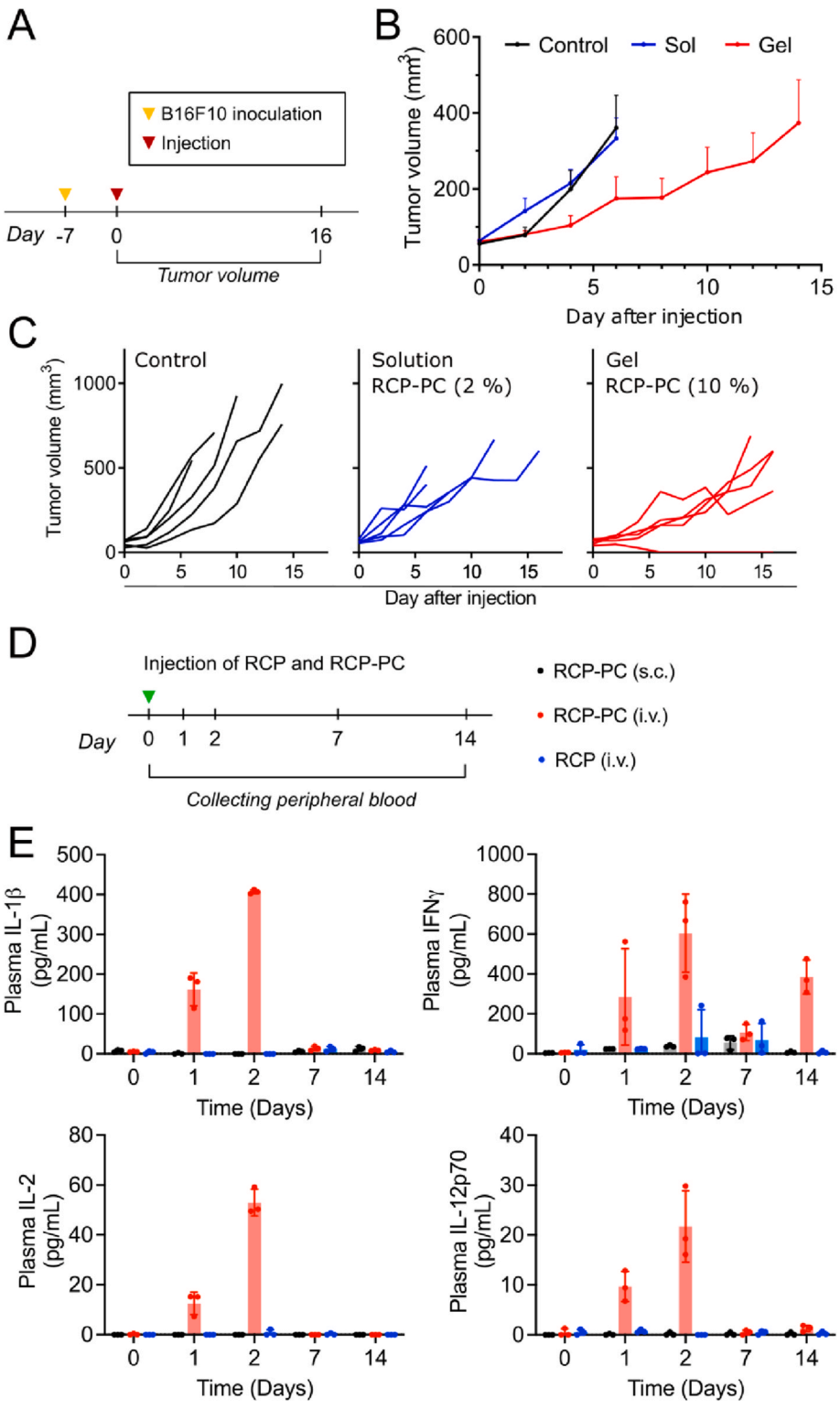

Fig. 6. Increased anti-tumor effects and inhibited over-inflammatory side effects of Ag/Adjuvant releases. A) Schematic illustration of schedule for anti-tumor therapeutic effect of the RCP-P hydrogel (10 %, 20 μL) and solution (2 %, 100 μL) in a B16F10 melanoma tumor model (RCP polymer 2 mg, PTX 20 μg per mouse, PBS as control). B) Tumor volume changes until day 14. n = 5 biologically independent animals per group. C) The individual tumor volumes until day 16, and numbers on the top side represent the number of survived mice. D) Schematic illustration of schedule for the administration of the RCP-PC (s.c and i.v.) and RCP (i.v.), mice peripheral blood collecting and analysis. E) The mice plasma level of inflammatory cytokines including IL-1β, IFNγ, IL-12p70, and IL-2 from day 0 (before administration) to day 14 (n = 3).

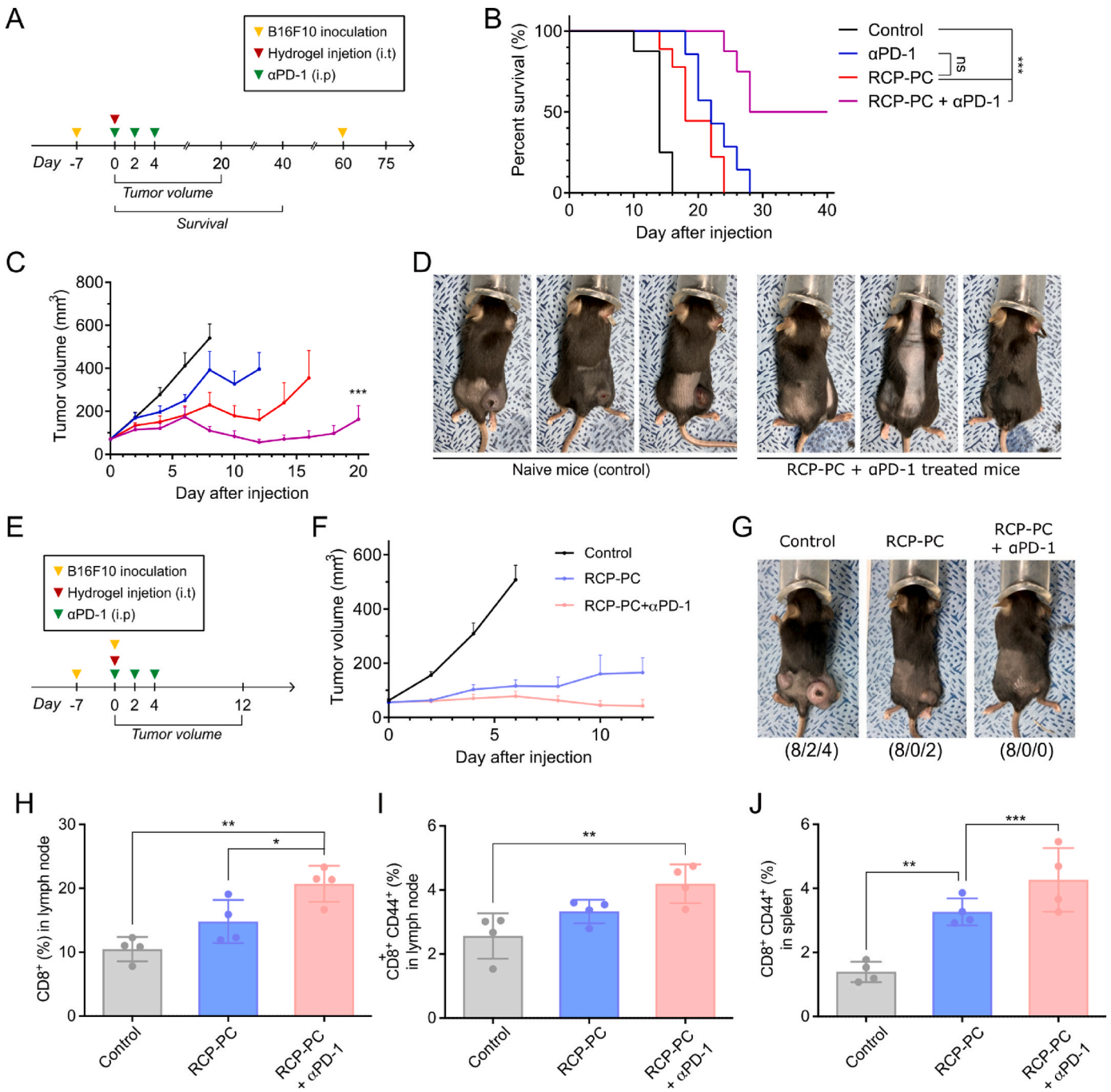

Fig. 7. Synergistic effect with *α*PD-1 by immune modulation and systemic immune activation-based inhibition of recurrence. A) Schematic illustration of schedule for the combined therapeutic procedure of the RCP hydrogel system with *α*PD-1 on B16F10. B) Survival rates represent Kaplan–Meier plots for all groups (n = 8). C) Tumor volume changes until day 20. D) The photographs of reinoculated B16F10 tumor in cured mice by RCP-PC with *α*PD-1 at day 75 following initiation of treatment. E) Treatment schedule for systemic anti-tumor immune response by RCP-PC with *α*PD-1. F) Primary tumor volume changes until day 20; n = 8 biologically independent animals per group. G) Representative images of mice at 10 days after intratumoral injection; numbers below the image represent the number of total mice/the number of dead mice/the number of mice that developed secondary tumors. H) Percentages of $CD8^+$ T cells in TDLNs (n = 4), I) memory T cells in TDLNs (n = 4), and J) memory T cells in spleens (n = 4) on day 12 after the injection of RCP-PC. * **, and *** indicate $P < 0.05$, $P < 0.01$, and $P < 0.001$, respectively, by one-way ANOVA followed by Tukey's post hoc analysis.

immune responses by maintaining the activity of memory T cells against B16F10 tumors.

4. Conclusion

In summary, we designed and synthesized an injectable, thermosensitive, and biodegradable hydrogel system for *in situ* cancer vaccines. This system can deliver ICD inducers and adjuvant-incorporated nanocomplexes to cancer cells and APCs, respectively, for extended periods with a single intratumoral administration.

The RCP-based NGN system demonstrates efficacy in modulating suppressive TIMEs into activated forms locally, with minimal systemic side effects, as follows. First, the NGN system can effectively load multiple drugs *via* hydrophobic/ionic interactions upon simple physical mixing. Furthermore, the slowly released nanocomplexes from the hydrogel are preferentially delivered to cancer cells *via* RGD-integrin-

mediated endocytosis, generating endogenous danger signals and TAAs from dying cancer cells. We also confirmed that the released nanocomplexes are suitable for intracellular uptake of adjuvants by APCs in the TIME, potentially inducing long-term immunity against tumor antigens. The sustained release of nano-sized polymeric complexes from the hydrogel *via* NGN can serve as an effective drug carrier system to elicit local immune responses. Moreover, the effective cellular uptake of nanocomplexes can reduce the dose of ICD inducers and adjuvants, minimizing systemic side effects while exerting favorable immune responses, including APC maturation and function [67]. Reprogramming the suppressive TIME using the NGN cancer vaccine system effectively inhibited tumor growth and enhanced the therapeutic response rates of ICBs in two different tumor models (B16F10 and CT26). Furthermore, we confirmed that combining the NGN and ICB elicited systemic and memory T cell responses, thereby inhibiting tumor recurrence and metastasis. This strategy not only elicited an appropriate immune response at the local site but also minimized undesired systemic inflammatory responses, such as cytokine storms, with only a single injection. As a result, it could become an alternative clinical approach to improve the patient's quality of life, avoiding surgical tumor removal or multiple systemic drug administrations. Further research avenues could involve inducing immune responses using other combinational drugs and improving preclinical outcomes by considering a wide range of doses of ICD inducers and adjuvants in the hydrogel.

Taken together, these results suggest that the NGN system could be utilized as a customized cancer immunotherapy platform with the potential to load other chemotherapeutic and immunotherapeutic drugs, depending on the type of cancer or the patient's condition. Furthermore, given its usefulness as a multi-drug carrier with simple formulation methods and selective delivery, it could be beneficial in a patient-friendly approach for the next generation of immune-related diseases with minimally invasive treatment.

Ethics approval and consent to participate

All investigations were performed at the Korea Institute of Science and Technology (KIST, Seoul, Republic of Korea). All animal-related protocols were approved by the Institutional Animal Care and Use Committee (IACUC) in the KIST and IACUC under approval (the approval number of 2022-112-6). Especially, the rodents for being inoculated for the cancer cells, C57BL/6 and Balb/c mice were supplied by a specialized animal company (Orient Bio, Seongnam, Republic of Korea).

CRediT authorship contribution statement

Sung Hoon Kim: Writing – original draft, Visualization, Methodology, Investigation, Data curation. **Rafael T. Han:** Methodology, Investigation, Data curation. **Hyung-Seop Han:** Writing – review & editing, Supervision, Investigation. **Young-Min Kim:** Writing – review & editing, Project administration, Investigation, Formal analysis, Conceptualization.

Declaration of competing interest

Hyung-Seop Han is an editorial board member for Bioactive Materials and was not involved in the editorial review or the decision to publish this article. All authors declare that there are no competing interests.

Acknowledgements

This research was supported by Korea Institute of Science and Technology (2E33151, Y.-M.K.). This work was supported by the Nano-Materials Technology Program (NRF-2021M3H4A1A04092879, 2022M3H4A1A04096393) funded by the Ministry of Science and ICT (MSIT). The authors also thank M.S. Kyungwoo Lee for his illustration and Dr. Seung Ja Oh, Dr. Hong Yeol Yoon and Yuna Cheon for their fruitful discussions on this work.

Appendix A. Supplementary data

Supplementary data to this article can be found online at https://doi.org/10.1016/j.bioactmat.2024.08.047.

References

[1] I. Mellman, G. Coukos, G. Dranoff, Cancer immunotherapy comes of age, Nature 480 (7378) (2011) 480–489.
[2] S.L. Topalian, G.J. Weiner, D.M. Pardoll, Cancer immunotherapy comes of age, J. Clin. Oncol. 29 (36) (2011) 4828.
[3] M.J. Smyth, S.F. Ngiow, A. Ribas, M.W. Teng, Combination cancer immunotherapies tailored to the tumour microenvironment, Nat. Rev. Clin. Oncol. 13 (3) (2016) 143–158.
[4] F.S. Hodi, S.J. O'day, D.F. McDermott, R.W. Weber, J.A. Sosman, J.B. Haanen, R. Gonzalez, C. Robert, D. Schadendorf, J.C. Hassel, et al., Improved survival with ipilimumab in patients with metastatic melanoma, N. Engl. J. Med. 363 (8) (2010) 711–723.
[5] S.L. Topalian, C.G. Drake, D.M. Pardoll, Immune checkpoint blockade: a common denominator approach to cancer therapy, Cancer Cell 27 (4) (2015) 450–461.
[6] L. Milling, Y. Zhang, D.J. Irvine, Delivering safer immunotherapies for cancer, Adv. Drug Deliv. Rev. 114 (2017) 79–101.
[7] A. Ribas, J.D. Wolchok, Cancer immunotherapy using checkpoint blockade, Science 359 (6382) (2018) 1350–1355.
[8] J.B. Haanen, Converting cold into hot tumors by combining immunotherapies, Cell 170 (6) (2017) 1055–1056.
[9] M. Binnewies, E.W. Roberts, K. Kersten, V. Chan, D.F. Fearon, M. Merad, L. M. Coussens, D.I. Gabrilovich, S. Ostrand-Rosenberg, C.C. Hedrick, et al., Understanding the tumor immune microenvironment (time) for effective therapy, Nat. Med. 24 (5) (2018) 541–550.
[10] P.D. Katsikis, K.J. Ishii, C. Schliehe, Challenges in developing personalized neoantigen cancer vaccines, Nat. Rev. Immunol. (2023) 1–15.
[11] S.A. Rosenberg, J.C. Yang, N.P. Restifo, Cancer immunotherapy: moving beyond current vaccines, Nat. Med. 10 (9) (2004) 909–915.
[12] M. Saxena, S.H. van der Burg, C.J. Melief, N. Bhardwaj, Therapeutic cancer vaccines, Nat. Rev. Cancer 21 (6) (2021) 360–378.
[13] O.J. Finn, Cancer vaccines: between the idea and the reality, Nat. Rev. Immunol. 3 (8) (2003) 630–641.
[14] S.-Y. Kim, Y.-W. Noh, T.H. Kang, J.-E. Kim, S. Kim, S.H. Um, D.-B. Oh, Y.-M. Park, Y.T. Lim, Synthetic vaccine nanoparticles target to lymph node triggering enhanced innate and adaptive antitumor immunity, Biomaterials 130 (2017) 56–66.
[15] C. Pfirschke, C. Engblom, S. Rickelt, V. Cortez-Retamozo, C. Garris, F. Pucci, T. Yamazaki, V. Poirier-Colame, A. Newton, Y. Redouane, et al., Immunogenic chemotherapy sensitizes tumors to checkpoint blockade therapy, Immunity 44 (2) (2016) 343–354.
[16] H. Wang, A.J. Najibi, M.C. Sobral, B.R. Seo, J.Y. Lee, D. Wu, A.W. Li, C.S. Verbeke, D.J. Mooney, Biomaterial-based scaffold for in situ chemo-immunotherapy to treat poorly immunogenic tumors, Nat. Commun. 11 (1) (2020) 5696.
[17] L. Zitvogel, O. Kepp, G. Kroemer, Immune parameters affecting the efficacy of chemotherapeutic regimens, Nat. Rev. Clin. Oncol. 8 (3) (2011) 151–160.
[18] T. Zhao, Y. Cai, Y. Jiang, X. He, Y. Wei, Y. Yu, X. Tian, Vaccine adjuvants: mechanisms and platforms, Signal Transduct. Targeted Ther. 8 (1) (2023) 283.
[19] H. Phuengkham, C. Song, Y.T. Lim, A designer scaffold with immune nanoconverters for reverting immunosuppression and enhancing immune checkpoint blockade therapy, Adv. Mater. 31 (42) (2019) 1903242.
[20] M.J. Smith, A.C. Culhane, S. Killeen, M.A. Kelly, J.H. Wang, T.G. Cotter, H. P. Redmond, Mechanisms driving local breast cancer recurrence in a model of breast-conserving surgery, Ann. Surg Oncol. 15 (2008) 2954–2964.
[21] O. Al-Sahaf, J.H. Wang, T.J. Browne, T.G. Cotter, H.P. Redmond, Surgical injury enhances the expression of genes that mediate breast cancer metastasis to the lung, Ann. Surg. 252 (6) (2010) 1037–1043.
[22] K. Park, Controlled drug delivery systems: past forward and future back, J. Contr. Release 190 (2014) 3–8.
[23] I. Melero, E. Castanon, M. Alvarez, S. Champiat, A. Marabelle, Intratumoural administration and tumour tissue targeting of cancer immunotherapies, Nat. Rev. Clin. Oncol. 18 (9) (2021) 558–576.
[24] D. Shae, J.J. Baljon, M. Wehbe, P.P. Christov, K.W. Becker, A. Kumar, N. Suryadevara, C.S. Carson, C.R. Palmer, F.C. Knight, et al., Co-delivery of peptide neoantigens and stimulator of interferon genes agonists enhances response to cancer vaccines, ACS Nano 14 (8) (2020) 9904–9916.
[25] Y.-M. Kim, S.-C. Song, Targetable micelleplex hydrogel for long-term, effective, and systemic sirna delivery, Biomaterials 35 (27) (2014) 7970–7977.
[26] Y.S. Sohn, Y.H. Cho, H. Baek, O.-S. Jung, Synthesis and properties of low molecular weight polyphosphazenes, Macromolecules 28 (22) (1995) 7566–7568.
[27] S. Osawa, T. Ishii, H. Takemoto, K. Osada, K. Kataoka, A facile amino-functionalization of poly (2-oxazoline) s' distal end through sequential azido end-capping and staudinger reactions, Eur. Polym. J. 88 (2017) 553–561.

[28] C. Chun, H.J. Lim, K.-Y. Hong, K.-H. Park, S.-C. Song, The use of injectable, thermosensitive poly (organophosphazene)–rgd conjugates for the enhancement of mesenchymal stem cell osteogenic differentiation, Biomaterials 30 (31) (2009) 6295–6308.
[29] J. Kim, B.-B. Seo, K.H. Hong, S.E. Kim, Y.-M. Kim, S.-C. Song, Long-term anti-inflammatory effects of injectable celecoxib nanoparticle hydrogels for achilles tendon regeneration, Acta Biomater. 144 (2022) 183–194.
[30] T. Potta, C. Chun, S.-C. Song, Dual cross-linking systems of functionally photo-cross-linkable and thermoresponsive polyphosphazene hydrogels for biomedical applications, Biomacromolecules 11 (7) (2010) 1741–1753.
[31] T. Potta, C. Chun, S.-C. Song, Rapid photocrosslinkable thermoresponsive injectable polyphosphazene hydrogels, Macromol. Rapid Commun. 31 (24) (2010) 2133–2139.
[32] G. Toda, T. Yamauchi, T. Kadowaki, K. Ueki, Preparation and culture of bone marrow-derived macrophages from mice for functional analysis, STAR protocols 2 (1) (2021) 100246.
[33] J. Helft, J. Böttcher, P. Chakravarty, S. Zelenay, J. Huotari, B.U. Schraml, D. Goubau, C.R. e Sousa, Gm-csf mouse bone marrow cultures comprise a heterogeneous population of cd11c+ mhcii+ macrophages and dendritic cells, Immunity 42 (6) (2015) 1197–1211.
[34] L.T.A. Hong, Y.-M. Kim, H.H. Park, D.H. Hwang, Y. Cui, E.M. Lee, S. Yahn, J.K. Lee, S.-C. Song, B.G. Kim, An injectable hydrogel enhances tissue repair after spinal cord injury by promoting extracellular matrix remodeling, Nat. Commun. 8 (1) (2017) 533.
[35] B.H. Lee, S.-C. Song, Synthesis and characterization of biodegradable thermosensitive poly (organophosphazene) gels, Macromolecules 37 (12) (2004) 4533–4537.
[36] Y.-M. Kim, M.-R. Park, S.-C. Song, Injectable polyplex hydrogel for localized and long-term delivery of sirna, ACS Nano 6 (7) (2012) 5757–5766.
[37] B.H. Lee, Y.M. Lee, Y.S. Sohn, S.-C. Song, A thermosensitive poly (organophosphazene) gel, Macromolecules 35 (10) (2002) 3876–3879.
[38] B.-B. Seo, H. Choi, J.-T. Koh, S.-C. Song, Sustained bmp-2 delivery and injectable bone regeneration using thermosensitive polymeric nanoparticle hydrogel bearing dual interactions with bmp-2, J. Contr. Release 209 (2015) 67–76.
[39] Z.-Q. Zhang, S.-C. Song, Thermosensitive/superparamagnetic iron oxide nanoparticle-loaded nanocapsule hydrogels for multiple cancer hyperthermia, Biomaterials 106 (2016) 13–23.
[40] J.H. Kim, J.-H. Lee, K.-S. Kim, K. Na, S.-C. Song, J. Lee, H.-J. Kuh, Intratumoral delivery of paclitaxel using a thermosensitive hydrogel in human tumor xenografts, Arch Pharm. Res. (Seoul) 36 (2013) 94–101.
[41] Y.-M. Kim, C.-H. Kim, S.-C. Song, Injectable ternary nanocomplex hydrogel for long-term chemical drug/gene dual delivery, ACS Macro Lett. 5 (3) (2016) 297–300.
[42] E.A. Verderio, D. Telci, A. Okoye, G. Melino, M. Griffin, A novel rgd-independent cell adhesion pathway mediated by fibronectin-bound tissue transglutaminase rescues cells from anoikis, J. Biol. Chem. 278 (43) (2003) 42604–42614.
[43] I.N. Kurniasih, H. Liang, P.C. Mohr, G. Khot, J.P. Rabe, A. Mohr, Nile red dye in aqueous surfactant and micellar solution, Langmuir 31 (9) (2015) 2639–2648.
[44] H. Sun, W. Hu, Y. Yan, Z. Zhang, Y. Chen, X. Yao, L. Teng, X. Wang, D. Chai, J. Zheng, et al., Using pamps and damps as adjuvants in cancer vaccines, Hum. Vaccines Immunother. 17 (12) (2021) 5546–5557.
[45] M. Jiang, J. Zeng, L. Zhao, M. Zhang, J. Ma, X. Guan, W. Zhang, Chemotherapeutic drug-induced immunogenic cell death for nanomedicine-based cancer chemo-immunotherapy, Nanoscale 13 (41) (2021) 17218–17235.
[46] Z. Li, X. Lai, S. Fu, L. Ren, H. Cai, H. Zhang, Z. Gu, X. Ma, K. Luo, Immunogenic cell death activates the tumor immune microenvironment to boost the immunotherapy efficiency, Adv. Sci. 9 (22) (2022) 2201734.
[47] J. Guo, Z. Yu, D. Sun, Y. Zou, Y. Liu, L. Huang, Two nanoformulations induce reactive oxygen species and immunogenetic cell death for synergistic chemo-immunotherapy eradicating colorectal cancer and hepatocellular carcinoma, Mol. Cancer 20 (1) (2021) 1–17.
[48] T.S. Lau, L.K.Y. Chan, G.C.W. Man, C.H. Wong, J.H.S. Lee, S.F. Yim, T.H. Cheung, I. A. McNeish, J. Kwong, Paclitaxel induces immunogenic cell death in ovarian cancer via tlr4/ikk2/snare-dependent exocytosis, Cancer Immunol. Res. 8 (8) (2020) 1099–1111.
[49] K.J. Pahk, C.-H. Shin, I.Y. Bae, Y. Yang, S.-H. Kim, K. Pahk, H. Kim, S.J. Oh, Boiling histotripsy-induced partial mechanical ablation modulates tumour microenvironment by promoting immunogenic cell death of cancers, Sci. Rep. 9 (1) (2019) 9050.
[50] J. Fucikova, R. Spisek, G. Kroemer, L. Galluzzi, Calreticulin and cancer, Cell Res. 31 (1) (2021) 5–16.
[51] M. Obeid, A. Tesniere, F. Ghiringhelli, G.M. Fimia, L. Apetoh, J.-L. Perfettini, M. Castedo, G. Mignot, T. Panaretakis, N. Casares, et al., Calreticulin exposure dictates the immunogenicity of cancer cell death, Nat. Med. 13 (1) (2007) 54–61.
[52] M.P. Cervantes-Silva, S.L. Cox, A.M. Curtis, Alterations in mitochondrial morphology as a key driver of immunity and host defence, EMBO Rep. 22 (9) (2021) e53086.
[53] E. Andreakos, R. Williams, J. Wales, B. Foxwell, M. Feldmann, Activation of nf-κb by the intracellular expression of nf-κb-inducing kinase acts as a powerful vaccine adjuvant, Proc. Natl. Acad. Sci. USA 103 (39) (2006) 14459–14464.
[54] G. Lalle, J. Twardowski, Y. Grinberg-Bleyer, Nf-κb in cancer immunity: friend or foe? Cells 10 (2) (2021) 355.
[55] S.-Y. Kim, S. Kim, J.-E. Kim, S.N. Lee, I.W. Shin, H.S. Shin, S.M. Jin, Y.-W. Noh, Y. J. Kang, Y.S. Kim, et al., Lyophilizable and multifaceted toll-like receptor 7/8 agonist-loaded nanoemulsion for the reprogramming of tumor microenvironments and enhanced cancer immunotherapy, ACS Nano 13 (11) (2019) 12671–12686.
[56] C.B. Rodell, S.P. Arlauckas, M.F. Cuccarese, C.S. Garris, R. Li, M.S. Ahmed, R. H. Kohler, M.J. Pittet, R. Weissleder, Tlr7/8-agonist-loaded nanoparticles promote the polarization of tumour-associated macrophages to enhance cancer immunotherapy, Nat. Biomed. Eng. 2 (8) (2018) 578–588.
[57] M. Ovais, M. Guo, C. Chen, Tailoring nanomaterials for targeting tumor-associated macrophages, Adv. Mater. 31 (19) (2019) 1808303.
[58] C.W. Wanderley, D.F. Colon, J.P.M. Luiz, F.F. Oliveira, P.R. Viacava, C.A. Leite, J. A. Pereira, C.M. Silva, C.R. Silva, R.L. Silva, et al., Paclitaxel reduces tumor growth by reprogramming tumor-associated macrophages to an m1 profile in a tlr4-dependent manner, Cancer Res. 78 (20) (2018) 5891–5900.
[59] N.P. Restifo, M.E. Dudley, S.A. Rosenberg, Adoptive immunotherapy for cancer: harnessing the t cell response, Nat. Rev. Immunol. 12 (4) (2012) 269–281.
[60] A.M. Krieg, Cpg motifs in bacterial dna and their immune effects, Annu. Rev. Immunol. 20 (1) (2002) 709–760.
[61] J. Wei, D. Wu, S. Zhao, Y. Shao, Y. Xia, D. Ni, X. Qiu, J. Zhang, J. Chen, F. Meng, et al., Immunotherapy of malignant glioma by noninvasive administration of tlr9 agonist cpg nano-immunoadjuvant, Adv. Sci. 9 (13) (2022) 2103689.
[62] Z. Xiong, L. Sun, H. Yang, Z. Xiao, Z. Deng, Q. Li, C. Wang, F. Shen, Z. Liu, Ni-alginate hydrogel microspheres with sustained interleukin 2 release to boost cytokine-based cancer immunotherapy, Adv. Funct. Mater. 33 (7) (2023) 2211423.
[63] G. Deng, Z. Sun, S. Li, X. Peng, W. Li, L. Zhou, Y. Ma, P. Gong, L. Cai, Cell-membrane immunotherapy based on natural killer cell membrane coated nanoparticles for the effective inhibition of primary and abscopal tumor growth, ACS Nano 12 (12) (2018) 12096–12108.
[64] M. Chavez, M.T. Silvestrini, E.S. Ingham, B.Z. Fite, L.M. Mahakian, S.M. Tam, A. Ilovitsh, A.M. Monjazeb, W.J. Murphy, N.E. Hubbard, et al., Distinct immune signatures in directly treated and distant tumors result from tlr adjuvants and focal ablation, Theranostics 8 (13) (2018) 3611.
[65] C.G. Park, C.A. Hartl, D. Schmid, E.M. Carmona, H.-J. Kim, M.S. Goldberg, Extended release of perioperative immunotherapy prevents tumor recurrence and eliminates metastases, Sci. Transl. Med. 10 (433) (2018) eaar1916.
[66] M.H. Spitzer, Y. Carmi, N.E. Reticker-Flynn, S.S. Kwek, D. Madhireddy, M. M. Martins, P.F. Gherardini, T.R. Prestwood, J. Chabon, S.C. Bendall, et al., Systemic immunity is required for effective cancer immunotherapy, Cell 168 (3) (2017) 487–502.
[67] H. Zhong, B. Han, I.L. Tourkova, A. Lokshin, A. Rosenbloom, M.R. Shurin, G. V. Shurin, Low-dose paclitaxel prior to intratumoral dendritic cell vaccine modulates intratumoral cytokine network and lung cancer growth, Clin. Cancer Res. 13 (18) (2007) 5455–5462.